iScience

Article

Subcellular targets and recognition mechanism of *Ralstonia solanacearum* effector RipE1

Graphical abstract

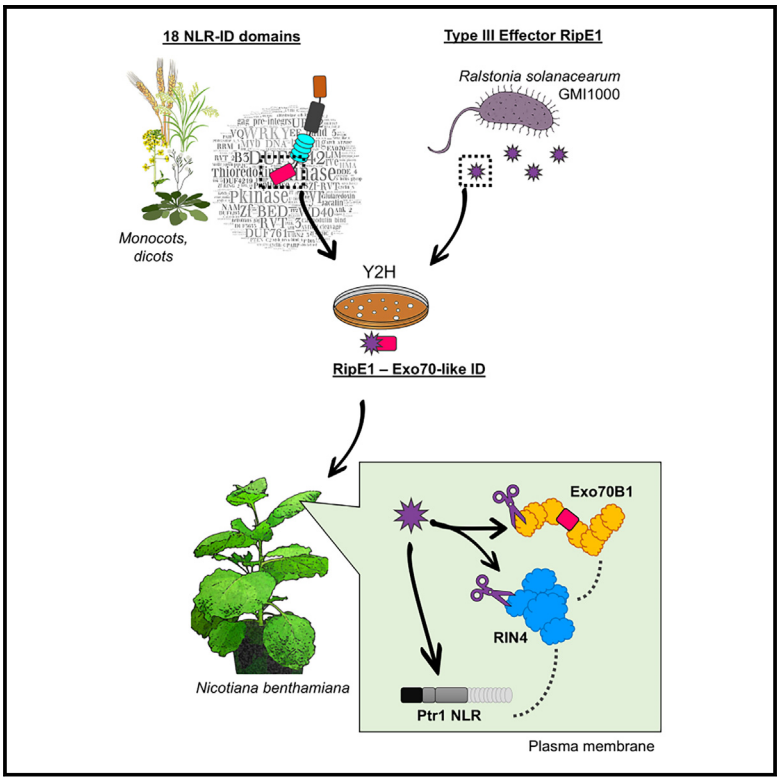

Highlights

- NLR-IDs are a potent tool in screening for putative effector subcellular targets
- *Ralstonia solanacearum* effector RipE1 has multiple putative targets and resides at the PM
- Cysteine protease RipE1 targets membrane trafficking components Exo70B1 and RIN4
- RipE1 activity is recognized by a RIN4-guarding NLR in *Nicotiana benthamiana*

Authors

Dimitra Tsakiri, Konstantinos Kotsaridis, Vassiliki A. Michalopoulou, ..., Michael Kokkinidis, Gregory B. Martin, Panagiotis F. Sarris

Correspondence

p.sarris@imbb.forth.gr

In brief

Natural sciences; Biological sciences; Molecular biology; Plant biology; Molecular plant pathology; Plant pathology

Tsakiri et al., 2025, iScience *28*, 112307
May 16, 2025
https://doi.org/10.1016/j.isci.2025.112307

CellPress

iScience

CellPress
OPEN ACCESS

Article

Subcellular targets and recognition mechanism of *Ralstonia solanacearum* effector RipE1

Dimitra Tsakiri,[1] Konstantinos Kotsaridis,[1] Vassiliki A. Michalopoulou,[1,2] Ning Zhang,[3,4] Sotiris Marinos,[1] Nikos Kountourakis,[2] Michael Kokkinidis,[1,2] Gregory B. Martin,[3,4] and Panagiotis F. Sarris[1,2,5,6,*]

[1]Department of Biology, University of Crete, 714 09 Heraklion, Crete, Greece
[2]Institute of Molecular Biology and Biotechnology, Foundation for Research and Technology-Hellas, 714 09 Heraklion, Crete, Greece
[3]Boyce Thompson Institute for Plant Research, Ithaca, NY 14853, USA
[4]Plant Pathology and Plant-Microbe Biology Section, School of Integrative Plant Science, Cornell University, Ithaca, NY 14853, USA
[5]Biosciences, University of Exeter, Exeter, Devon EX4 4SB, UK
[6]Lead contact
*Correspondence: p.sarris@imbb.forth.gr
https://doi.org/10.1016/j.isci.2025.112307

SUMMARY

Some plant NLRs carry unusual integrated protein domains (IDs) that mimic host targets of pathogen effectors. RipE1 is a core *Ralstonia solanacearum* Type III effector with a predicted cysteine protease activity that activates defense responses in resistant plants. In this study, we used a library of NLR-IDs as an investigative tool to screen for potential host-cell targets of RipE1. Based on these findings and the effector's localization, we identified two plant membrane trafficking components as RipE1's subcellular targets. Depending on its protease activity, RipE1 promotes the degradation of both exocyst complex subunit Exo70B1 and its known interactor RPM1-interacting protein-4 (RIN4), a known plant immunity regulator. RipE1 protease activity is recognized by the RIN4-guarding NLR *Pseudomonas* tomato race 1 (Ptr1) in *Nicotiana benthamiana*. Overall, the data presented here, along with the existing literature, suggest a possible link between RipE1 activity upon the host secretion machinery and its NLR-mediated recognition.

INTRODUCTION

Plants, unlike animals, rely solely on their innate immune system to activate defense responses and fight off pathogens.[1,2] To counter these responses, pathogens have evolved multiple virulence components, also known as effectors, that manipulate their host's eukaryotic cell metabolism, including pathways involved in innate immunity.[3–5] Plant innate immunity involves two intertwined cross-talking pathways that discern signs of invasion, namely pattern-triggered immunity (PTI) and effector-triggered immunity (ETI).[6,7] During ETI, pathogen effectors translocated inside the host cell are recognized by plant intracellular nucleotide-binding leucine-rich repeat receptors (NLRs).[8,9] Effector recognition often leads to the induction of a localized rapid programmed cell death, known as the hypersensitive response (HR), that stops pathogen spread.[10,11] NLRs can recognize effectors either by directly binding them or by indirectly perceiving effector-caused modifications on target plant proteins.[12,13] A specialized version of direct recognition by NLRs is mediated by protein domains integrated on NLRs (NLR-IDs).[12,14,15] This model refers to NLRs carrying non-canonical domain fusions (integrated domains – IDs) that resemble pathogen targets to attract effectors and facilitate recognition.[14,15] Since NLR IDs mimic conserved domains of various eukaryotic protein families and appear to significantly overlap with known effector subcellular targets, they are a potent investigative tool for studying effector function.[14,16]

Components of plant membrane trafficking pathways play a major role in the sophisticated coordination of plant defense responses.[17] Among them, the exocyst is an octameric protein complex that mediates the tethering of secretory vesicles to the plasma membrane.[18,19] Although the same eight subunits -Sec3, Sec5, Sec6, Sec8, Sec10, Sec15, Exo70, and Exo84- comprise the so-far characterized exocyst complexes from different organisms, multiple paralogues encode several of the plant exocyst subunits, with Exo70 paralogues being the most abundant.[20–22] Specifically, the role of Arabidopsis Exo70B1 in plant defense is highlighted not only by its interaction with key regulators and immune receptors but also by the fact that different pathogen effectors target Exo70B1, aiming to disrupt the host secretion of defense-related molecules.[23–27] Expanding evidence also links Exo70B1 and other exocyst components to RPM1-interacting protein 4 (RIN4),[26,28–30] an immunity regulator also targeted by multiple pathogen effectors and monitored by convergently evolved NLRs from different plant species.[31–35] Given the suspected regulatory role of RIN4 association with membrane trafficking components, such complexes could potentially be targeted by pathogens, as it has been independently shown for effector AvrPtoB from *Pseudomonas syringae*.[23,36]

Ralstonia solanacearum is a destructive plant pathogen and the causative agent of bacterial wilt disease, affecting more than 250 plant species, including agronomically important

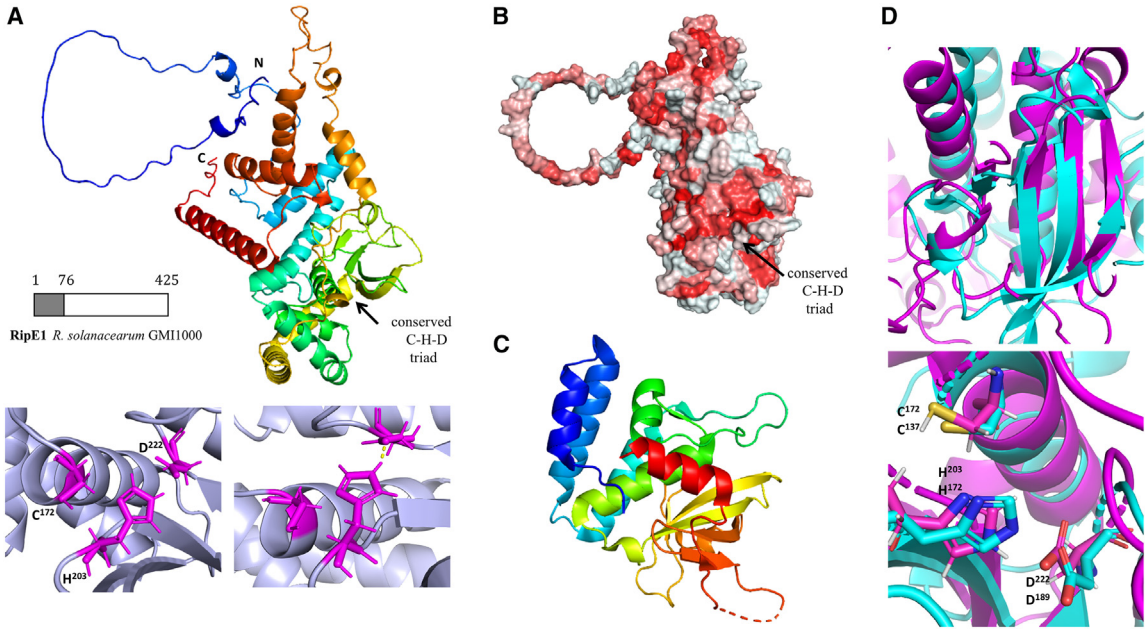

Figure 1. RipE1 protein structure *in silico* prediction supports a cysteine protease folding

(A) Schematic presentation of 3D structure prediction of *Ralstonia solanacearum* GMI1000 effector RipE1, using AlphaFold Colab (N-terminal is shown in blue, C-terminal is shown in red). The first 76 residues were predicted as unfolded. The conserved catalytic triad (Cys-His-Asp, C172-H203-D222) and the hydrogen bond between H203 and D222 are shown bottom left.

(B) Surface hydrophobicity of RipE1 predicted structure. Hydrophobic surfaces appear in red.

(C) Crystal structure of *Legionella pneumophila* cysteine protease LapG (N-terminal is shown in blue, C-terminal is shown in red).

(D) Superimposition of the active sites of the two proteins: LapG (cyan) residues C137, H172, and D189 and RipE1 (magenta) residues C172, H203, and D222.

crops.[37,38] As in the case of many Gram-negative bacterial pathogens, *R. solanacearum* Type III Secretion System (T3SS) is considered as a key virulence mechanism, injecting more than 70 Type III Effectors (T3Es) inside the host cell to promote colonization.[37,39,40] RipE1 is a highly conserved T3E among the so far sequenced strains of the *R. solanacearum* species complex, with a predicted protease activity.[39–41] Recent data suggest the effector's contribution to virulence, the fact that it triggers defense responses in model plant species, as well as evidence that other *R. solanacearum* T3Es are potentially able to suppress these responses.[41–45]

In this work we aimed to uncover new host targets of RipE1 and further investigate the molecular mechanism that guides its activity and recognition in model plant species. We utilized a yeast two-hybrid screening library of NLR-IDs to identify putative RipE1 host targets. Although this screening revealed multiple potential RipE1 targets, we focused on its association with an Exo70-like domain, in accordance with the effector's subcellular localization in planta. Hence, we uncover exocyst component Exo70B1 and the known exocyst interactor RPM1-interacting protein 4 (RIN4) as subcellular targets of RipE1. AI-based effector structure and function predictions, as well as experimental evidence, suggest that RipE1 promotes the degradation of Exo70B1 and RIN4, depending on its cysteine protease activity. The subcellular RipE1 targets revealed in this study, along with the existing literature, led to the investigation of a previously characterized RIN4-guarding CC-NLR, named *Pseudomonas* tomato race 1 (Ptr1), as the NLR required for the effector's recognition and activation of cell death in *N. benthamiana*. Overall, this study presents an *R. solanacearum* effector targeting components of the host secretion machinery and grants tools and insights into discovering plant pathogen effectors' distinctive targets when aiming to investigate both virulence and avirulence mechanisms.

RESULTS AND DISCUSSION

RipE1 protein structure *in silico* prediction supports a cysteine protease folding

AlphaFold, developed by DeepMind, is an artificial intelligence (AI)-based protein structure prediction tool, which has been proposed as a highly accurate method to predict protein structures compared with other well-established methods.[46,47] Here, the 3D structure of RipE1 (47.31 kDa) was predicted using the AlphaFold Colab (Figure 1A). The resulted structure confirmed that RipE1 has a cysteine protease folding. Cysteine proteases (thiol proteases) are enzymes with the ability of protein degradation by the deprotonation of a thiol in the enzyme's active site.[48] Therefore, all enzymes in this category have a common catalytic triad or dyad involving a nucleophilic cysteine residue.[48] The predicted RipE1 structure was compared to Protein DataBank structures via the DALI online server.[49] The highest similarity was with the *Legionella pneumophila* periplasmic protease LapG[50] (Figure 1C). According to this comparison, the extending hydrophobic surface patch at the active site of RipE1 (Figure 1B) may suggest a role as an interaction interface for substrate

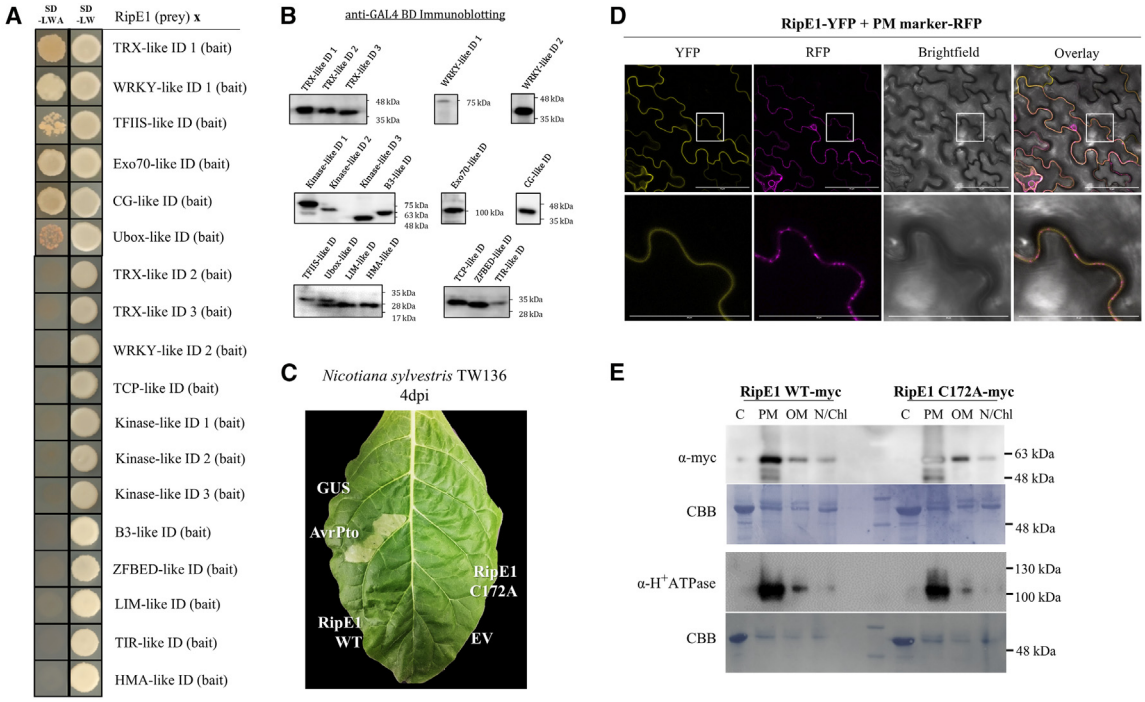

Figure 2. RipE1 has multiple putative subcellular targets and mainly localizes at the plasma membrane in plant cells

(A) A total of 18 NLR-IDs, originating from both dicot and monocot plant genomes, were used in a yeast two-hybrid screening to test their possible interaction with effector RipE1. Yeast cells carrying the indicated baits and preys were spotted on SDC-LW (plasmid selection) and SDC-LWA plates (interaction selection). Photographs were taken after 4 days of incubation. Each putative interaction was tested at least 3 times. Details about the sequence and origin of all NLR-IDs are provided in Table S1. Auto-activity yeast two-hybrid assays for the proteins that yielded positive results are presented in Figure S1A.

(B) Immunoblots using mouse-produced anti-GAL4 BD antibody verifying the expression of all 18 NLR-IDs used in the screening presented in Figure 2A. Information about the expected molecular weight of NLR-IDs fused to GAL4 DNA binding domain are provided in Table S1. CBB staining of the blots is shown in Figure S1B.

(C) RipE1 does not activate cell death in *Nicotiana sylvestris* TW136. Wild type RipE1 and its derived mutant C172A do not induce a hypersensitive response (HR) in *Nicotiana sylvestris* ecotype TW136. Effector AvrPto was used as a positive HR-inducing control, and the GUS reporter gene was used as a negative control. This photograph was taken 4 dpi. This experiment was repeated at least 6 times with the same exact results. Expression of proteins of interest was verified via immunoblotting (see Figure S1C).

(D) Subcellular localization of effector RipE1 in plant cells. RipE1-YFP and RFP fused to plasma membrane (PM) intrinsic protein 2A, which was used as a PM marker, were transiently expressed via *Agrobacterium*-mediated infiltration. Agroinfiltrated areas were observed via confocal microscopy and images were captured 48hpi. The boxed area in the top row panels were zoomed in, and the results are presented in the bottom row. Scale bars in the top panels are 70 μm, and in the bottom panels are 35 μm.

(E) Fractionation analysis of *N. sylvestris* tissue transiently expressing RipE1-myc and RipE1 C172A-myc at 3dpi. Immunoblot analysis with an anti-myc antibody verified localization of RipE1 mostly to the plasma membrane (PM), as well as to nuclear and chloroplastic (N/Chl) and organelle membrane (OM) fractions in smaller quantities. RipE1 was not detected in the cytoplasmic (C) fraction. This localization was independent of the effector's cysteine protease activity. Immunoblotting with an a-H+-ATPase antibody and CBB staining were performed to verify the proper fractionation.

binding. Subsequently, the superimposition (Figure 1D) of the active site domain between the two proteins had a root-mean-square deviation (RMSD) of 1.544. The catalytic triad cysteine-histidine-aspartate (C-H-D) of RipE1, specifically C172-H203-D222 (Figure 1A), appeared to be identical to the LapG C137-H172-D189 catalytic triad (Figure 1D). RipE1 belongs to the HopX1/AvrPphE effector family, the members of which share a conserved N-terminal domain and a catalytic triad with predicted cysteine protease activity.[51–53] RipE1 has been shown to possess cysteine protease activity *in vitro,* and it seemingly depends on it to cleave JAZ repressors.[41] Using AI-based structural predictions (Figure 1), we further support the notion that RipE1 is a cysteine protease. This additionally supports the findings of Sang et al.,[43] who reported that RipE1 loses its immunity-inducing attribute in *Nicotiana benthamiana* and *Arabidopsis thaliana* plants when the cysteine residue belonging to its catalytic triad is substituted. In addition, the first 76 amino acid residues (Figure 1A) of RipE1 appeared to be a disordered region. Although more research is required to determine if this region mediates protein-protein interactions, disordered protein regions could hint at the binding of multiple different protein partners.[54]

RipE1 has multiple putative subcellular targets, and it mainly localizes at the plasma membrane of plant cells

To identify new putative subcellular targets of RipE1, we performed a yeast two-hybrid (Y2H) screening between RipE1 and 18 eukaryotic protein domains (Figure 2A; Table S1) that are

fused to plant NLRs as Integrated Domains (NLR-IDs). The 18 different NLR-IDs in this library (Table S1) were selected for a variety of reasons: (1) they originate from both monocot and dicot plant species, (2) they contain well-conserved domains that characterize large plant protein families, (3) they are commonly found as NLR-IDs, (4) they are -to some extent-representative of host proteins often targeted by effectors.[14] Using this library, we uncovered a total of 6 interactions between RipE1 and IDs of various NLRs. Specifically, RipE1 interacted with a TRX-like, a WRKY-like, an Exo70-like, a CG-like and a TFIIS-like ID, while a weaker interaction was also detected between RipE1 and a Ubox-like domain of our ID collection (Figure 2A; Table S1). Neither the expression of either RipE1 or any of the IDs in yeast were not able to activate the reporter gene in the absence of an interactor, reducing the possibility of false-positive results in this screening (Figure S1A). Pathogen effectors often interfere with multiple host pathways to promote virulence,[4] and our results, along with the pre-existing literature, jointly point out that RipE1 seems to be implicated in several T3E functions.[24,41–43] While the number of interactions uncovered in this screening was surprising and could suggest unspecific binding of RipE1 to a multitude of targets, protein analysis from yeast transformants supported the specificity of the interactions (Figures 2B and S1B). For example, RipE1 only interacted with one out of two WRKY-like domains and with one out of three TRX-like domains from our list (Figures 2A, 2B, S1B, and Table S1). Our findings provide new putative RipE1 subcellular targets and we hope that they advance the discovery of more functions of this highly conserved *R. solanacearum* effector. To select the strongest candidate(s) for further investigation, we proceeded to study RipE1 subcellular localization *in planta*. Since RipE1 has been shown to trigger a hypersensitive response in *Nicotiana benthamiana*, *Nicotiana tabacum* and induce defense responses in *Arabidopsis thaliana*[42,43], we screened various *Nicotiana* species, including various *Nicotiana sylvestris* ecotypes, to find a new plant model for our experiments *in planta*. We discovered that RipE1 did not trigger an HR response when it was transiently expressed in leaves of *N. sylvestris* ecotype TW136 from our collection via *Agrobacterium*-mediated infiltration (Figures 2C and S1C). We used this ecotype as a novel tool to perform our thereupon *in-planta* experiments. RipE1 C-terminally tagged with YFP mainly localized to the cell periphery and co-localized with RFP fused to plasma membrane (PM) intrinsic protein 2A, which was used as a PM marker (Figure 2D). Furthermore, fractionation analysis of transiently expressed RipE1 and its derived mutant, carrying a C172A substitution at the active site (RipE1-C172A), revealed that the effector mainly resides at the PM independently of its cysteine protease activity (Figure 2E). These results are in line with the previously reported colocalization of RipE1 with the PRR FLS2.[55] Based on these observations, we selected the interaction between RipE1 and the Exo70-like ID as the strongest candidate for further investigation, aiming to uncover PM-associated subcellular targets of the effector.

RipE1 interacts with exocyst component Exo70B1 and partially activates ectopic TN2-mediated cell death

Based on our previously performed Blastp analysis using the Exo70-like ID as a query,[24] we identified the *Arabidopsis thaliana* exocyst protein *At*Exo70B1 as the most likely component to be targeted by RipE1. The Exo70-like ID used here belongs to the RGH2 NLR of *Hordeum vulgare* (Figure S1D; Table S1), whose C-terminal Exo70 domain is known to mostly resemble Exo70F1 protein. However, the Exo70-like ID in our library consists of an extended part of RGH2, containing the Exo70 pfam domain and a 341-aa region upstream of that (Figure S1D; Table S1). According to Blastp results of our analysis, this extended sequence mostly resembles Exo70B1 and their similarity in protein structure has been previously supported via *in silico* predictions.[47] Given that, we proceeded by testing the interaction between Arabidopsis Exo70B1 and RipE1 in yeast. As shown in Figure 3A, Exo70B1 not only interacted with RipE1, but also with two effector mutants, the RipE1-C172A and the RipE1-ΔA. The latter lacks eight conserved amino acids (121–128) of unknown function, found at the N-termini of different members of HopX1 effectors family, also collectively known as the A-box.[43,51] The two mutations were designed according to the structural predictions presented in Figure 1, but also due to their previously reported inability to induce plant immune responses in model plants.[43] Overall, these results suggest that *At*Exo70B1 is a putative subcellular target of RipE1 and we proceeded to further investigate this interaction *in planta*. To test the possible association of RipE1 and Exo70B1 *in planta*, we used a Bimolecular Fluorescent Complementation (BiFC) assay, transiently co-expressing RipE1 tagged with C-terminal YFP (cCFP) and Exo70B1 tagged with N-terminal YFP (nVenus) in *N. sylvestris* leaf tissue. YFP signal was detected at the PM of plant cells 48 hpi via confocal microscopy, as shown in Figures 3B and S2B, indicating the association between the two proteins *in planta*. We additionally performed co-immunoprecipitation (coIP) assays to validate the RipE1/Exo70B1 interaction. Exo70B1-hellfire (6xHis-3Xflag C-terminal epitope tag) pull-down did precipitate RipE1-myc and RipE1-C172A-myc after their *Agrobacterium*-mediated transient co-expression, supporting the association between the proteins in plant cells (Figure S2C). Co-localization analysis of *At*Exo70B1 and RipE1 and additional controls for BiFC assays are presented in Figures S2A and S2B. Since RipE1 has a predicted cysteine protease activity (Figure 1), we hypothesized that it might cleave *At*Exo70B1. There is strong evidence that Exo70B1 is guarded by the TN2 (TIR-NBS2) NLR in Arabidopsis in a CPK5 (Calcium-dependent Protein Kinase 5)-dependent manner and that Exo70B1 degradation induces NLR-mediated immune responses.[23,27,47,56] TN2 expression in *N. tabacum* triggers a strong cell death response, suppressed by co-expression with Exo70B1 and subsequently rescued by the *Pseudomonas syringae* effector AvrPtoB, which induces *At*Exo70B1 degradation.[23] Based on this information and on our findings so far, we hypothesized that possible *At*Exo70B1 degradation after cleavage by RipE1 would be able to induce TN2-dependent cell death response. We observed that TN2 also triggers a cell death response in *N. sylvestris,* which was successfully suppressed by co-expression with *At*Exo70B1 (Figures 3C and 3D). In accordance with our hypothesis, the co-expression of TN2 and Exo70B1 with RipE1 partially rescued TN2-mediated HR in *N. sylvestris* (Figure 3C), suggesting that RipE1 partially promotes *At*Exo70B1 degradation

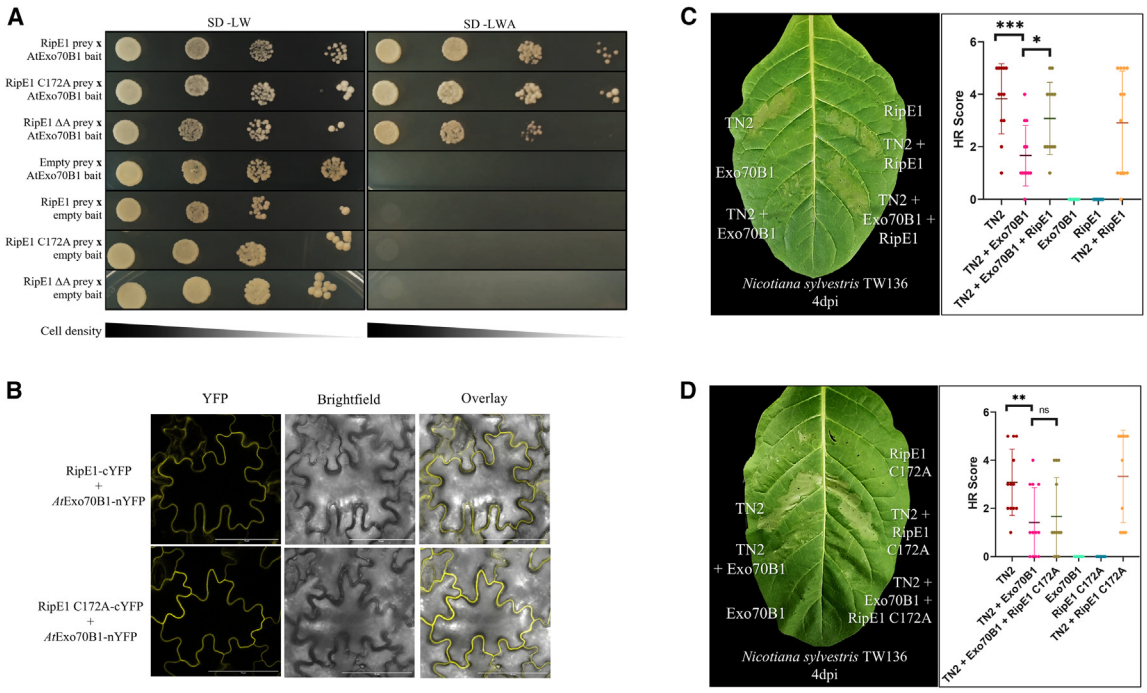

Figure 3. RipE1 interacts with Arabidopsis exocyst component Exo70B1 and partially activates ectopic TN2-mediated cell death

(A) Interactions between wild-type RipE1, RipE1-C172A mutant, RipE1 ΔA mutant, and *Arabidopsis thaliana* Exo70B1 in yeast. Serial dilutions of cells carrying the indicated baits and preys were spotted on SDC-LW and SDC-LWA selective plates. Initial OD_{600} of cells was 1 unit, and subsequent dilutions were made 0.1x, 0.01x, and 0.001x. Photographs were taken after 4 days of incubation.

(B) *In planta* validation of the RipE1/Exo70B1 (upper panels) and the RipE1 C172A/Exo70B1 (lower panels) association using BiFC assays in *N. sylvestris* plants. RipE1 and Exo70B1 were fused at their C-termini with cCFP (cYFP) and nVenus (nYFP) epitope tags, respectively, and the YFP signal was detected via confocal microscopy 48 hpi. Scale bars are 70 μm. Additional controls for this assay are provided in Figure S2B.

(C) Testing the ability of wild type RipE1 to rescue TN2-induced cell death phenotype via *At*Exo70B1 degradation. In the left panel, a *Nicotiana sylvestris* leaf represents one of the 12 biological replicates used for the statistical analysis of hypersensitive response (HR) assays presented in the right panel. The indicated proteins were transiently expressed via *Agrobacterium*-mediated infiltration at a total OD_{600} of 0.5. The photograph was captured at 3 dpi. To quantify the results of these experiments, HR scores representing cell death severity were first assigned to the observed phenotypes from 12 biological replicates. For the statistical analysis, assigned HR scores from all 12 replicates were then submitted to t-test followed by Welch's correction. ***p value = 0.0003, *p value = 0.0125.

(D) Testing the ability of mutated RipE1 C172A to rescue TN2-induced cell death phenotype via *At*Exo70B1 degradation. In the left panel, a *Nicotiana sylvestris* leaf represents one of the 12 biological replicates used for the statistical analysis of hypersensitive response (HR) assays presented in the right panel. The indicated proteins were transiently expressed via *Agrobacterium*-mediated infiltration at a total OD_{600} of 0.5. The photograph was captured at 3 dpi. To quantify the results of these experiments, HR scores representing cell death severity were first assigned to the observed phenotypes from 12 biological replicates. For the statistical analysis, assigned HR scores from all 12 replicates were then submitted to t-test followed by Welch's correction. **p value = 0.0085, ns: no significance p value = 0.6931.

in planta. When the RipE1-C172A mutant was used to perform similar assays, RipE1-C172A failed to rescue TN2-mediated HR similarly, indicating that this rescue is dependent on the effector's cysteine protease activity (Figure 3D). To expand our understanding of the interaction between *At*Exo70B1 and RipE1, we predicted and visualized the interaction *in silico* via AlphaFold, where we observed that the 146–201 aa region of *At*Exo70B1 appears to approach the catalytic triad of RipE1 (Figure S2E). In accordance, *in vitro* cleavage assays data showed that RipE1 can, in part, cleave *At*Exo70B1 *in vitro* (Figures S2D–S2G). TN2 activation could possibly cause the C172-dependent induction of immune responses by RipE1 in Arabidopsis, which has been previously reported by Sang et al.[43] In said study, the authors reported the induction of immunity-related marker genes after RipE1 expression in transgenic Arabidopsis plants, but they did not observe the activation of cell death.[43] Interestingly, in our experiments, although RipE1 was able to moderately activate TN2-dependent cell death when the receptor was ectopically expressed in *N. sylvestris* leaves (Figures 3C and 3D), transient expression of RipE1 in Arabidopsis Col-0 leaves failed to activate cell death (Figures S2H and S2I). Overall, these data indicate that, although *At*Exo70B1 can act as a substrate for RipE1, it may not be the primary effector target. In addition, to elucidate the mechanism by which RipE1 induces immune responses -but not cell death-in Arabidopsis, further knowledge is required regarding the regulation of TN2 expression and TN2-activated hypersensitive response. Since it was also previously reported that RipE1 causes C172-dependent cell death in *N. benthamiana*,[43] we decided to test if this observation is linked to RipE1 possibly targeting *Nb*Exo70B1 or other related proteins of this plant model.

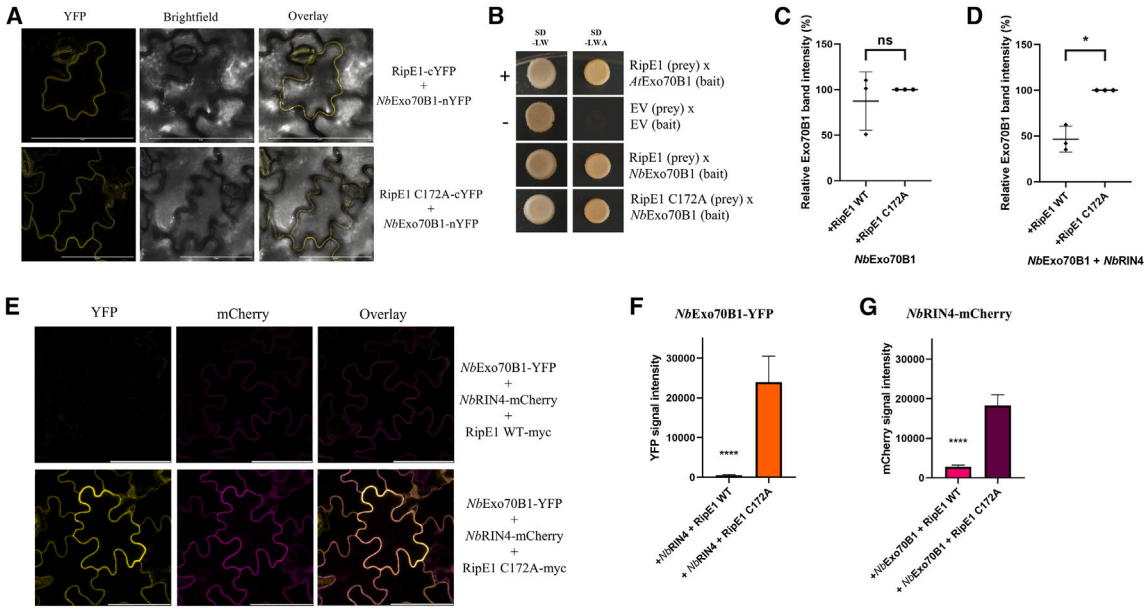

Figure 4. RipE1 interacts with *Nicotiana benthamiana* exocyst component Exo70B1 and promotes its degradation in the presence of RIN4

(A) *In planta* association of RipE1 and its derived mutant RipE1 C172A with *Nicotiana benthamiana* protein Exo70B1. Proteins of interest were fused at their C-termini with cCFP (cYFP) or nVenus (nYFP) epitope tags, as indicated, and the YFP signal was detected via confocal microscopy 48 hpi. Scale bars are 70 μm.

(B) Yeast two-hybrid assays to test the interaction between RipE1 and its derived mutant RipE1 C172A and *Nicotiana benthamiana* protein Exo70B1. Interaction between RipE1 and *At*Exo70B1 was used as a positive control. Yeast cells carrying the indicated baits and preys were spotted on SDC-LW and SDC-LWA selective plates. Photographs were taken after 4 days of incubation.

(C) Statistical analysis to examine the possible RipE1-promoted degradation of *N. benthamiana* Exo70B1, after their transient co-expression. Relative *Nb*Exo70B1 band intensity was measured via FiJi in the immunoblots from 3 biological replicates. *Nb*Exo70B1 protein levels in the presence of wild type RipE1 were compared to those in the presence of mutated RipE1 C172A as a means to detect any possible *Nb*Exo70B1 degradation caused by the catalytic activity of RipE1. For the statistical analysis, *Nb*Exo70B1 relative band intensity measurements from all 3 biological replicates were submitted to t-test followed by Welch's correction. ns: no significance p value = 0.5674. Representative immunoblot of this assay is presented in Figure S3B.

(D) Statistical analysis to examine the possible RipE1-promoted degradation of *N. benthamiana* Exo70B1, in the presence of *N. benthamiana* protein RIN4. Relative *Nb*Exo70B1 band intensity in immunoblot analysis was measured via FiJi in the immunoblots from 3 biological replicates. While co-expressed with *Nb*RIN4 in all cases, *Nb*Exo70B1 protein levels in the presence of wild type RipE1 were compared to those in the presence of mutated RipE1 C172A, as a means to detect any possible *Nb*Exo70B1 degradation caused by the catalytic activity of RipE1. For the statistical analysis, *Nb*Exo70B1 relative band intensity measurements from all 3 biological replicates were submitted to t-test followed by Welch's correction. *p value = 0.0225. Representative immunoblot of this assay is presented in Figure S3C.

(E) *N. benthamiana* proteins Exo70B1 and RIN4, fused at their C-termini with YFP or mCherry respectively, were transiently expressed in *N. sylvestris* leaves with wild type RipE1 or its derived mutant C172A, C-terminally tagged with the myc epitope. YFP and mCherry signal was detected via confocal microscopy at 3 dpi. Scale bars are 70 μm. RipE1-myc and RipE1 C172A-myc expression were verified by immunoblotting, as shown in Figure S3D.

(F) Statistical analysis of measured YFP signal in Figure 4E. YFP signal was measured in FiJi in a total of 15 ROIs and was compared in two cases: co-expression with either wild type RipE1 or its derived mutant C172A. Compared measurements were submitted to a t-test followed by Welch's correction. ****p value < 0.0001.

(G) Statistical analysis of measured mCherry signal in Figure 4E mCherry signal was measured in FiJi in a total of 15 ROIs and was compared in two cases: co-expression with either wild type RipE1 or its derived mutant C172A. Compared measurements were submitted to t-test followed by Welch's correction. ****p value < 0.0001.

RipE1 interacts with *Nicotiana benthamiana* exocyst component Exo70B1 and promotes its degradation in the presence of RPM1-interacting protein 4 (RIN4)

RipE1 could associate with *Nicotiana benthamiana* protein Exo70B1 both *in planta* (Figures 4A and S3A) and in yeast (Figure 4B), independently of its cysteine protease activity. Since we suspected *Nb*Exo70B1 to be a potential target of RipE1, we examined the possible RipE1-promoted degradation of *Nb*Exo70B1 *in planta*. RIN4 is an NO3-induced (NOI) domain-containing protein and a target of multiple effector proteins.[57] It is well-studied for its regulatory role in plant immunity, and it has been suggested to act as a hub for the formation of protein complexes.[57] It is noteworthy that accumulating evidence supports the association of RIN4 with Exo70B1 and other exocyst components[26,28–30] and that it has been previously shown to recruit Exo70B1 to the PM.[26] Considering this, we decided to investigate whether *Nb*Exo70B1 levels could be affected by RipE1 protease activity in the presence of *Nb*RIN4. After the transient overexpression of *Nb*Exo70B1 in *N. sylvestris* leaf tissue, along with the wild type or inactive RipE1, no significant difference was detected regarding *Nb*Exo70B1 protein levels in the presence of wild type RipE1, compared to the inactive mutant C172A (Figures 4C and S3B). Interestingly, when *Nb*RIN4 was also over-expressed, we observed significantly decreased *Nb*Exo70B1 levels in co-expression with wild type RipE1, compared to the levels co-expressed with the effector's inactive

mutant C172A (Figures 4D and S3C). In 2017, Sabol et al. reported that upon AvrRpt2 delivery, both RIN4 fragments and Exo70B1 are released from the PM to the cytoplasm.[26] Although these data support the hypothesis that RIN4 integrity is important for Exo70B1 localization to the PM, what happens to RIN4 in the case of Exo70B1 compromising has not been investigated. To investigate possible changes in protein localization, we transiently co-expressed *Nb*Exo70B1-YFP and *Nb*RIN4-mCherry, along with either RipE1 WT-myc (wild type) or RipE1 C172A-myc and observed the infiltrated tissue via confocal microscopy at 3 dpi. Interestingly, in the presence of wild type RipE1, although we did not observe changes in protein localization, we did detect a significant decrease in the signal of both YFP and mCherry (Figures 4E–4G and S3D). While this data further supports that RipE1 promotes *Nb*Exo70B1 degradation in the presence of *Nb*RIN4, it also raises the question of *Nb*RIN4 also being possibly targeted by the effector's protease activity.

RipE1 interacts with *Nicotiana benthamiana* RIN4 and promotes its degradation *in planta*, depending on RipE1 cysteine protease activity

In our earlier discussed results, the moderate nature of *At*Exo70B1 *in vitro* cleavage (Figure S2) and TN2 activation (Figures 3C and 3D) might suggest that Exo70B1 might not be the primary target of RipE1. In addition, RIN4 has been associated with multiple membrane trafficking components, and a *Pseudomonas syringae* effector, AvrPtoB, has been found to target both Exo70B1 and RIN4 for degradation.[23,36] To investigate the possibility of RipE1 predominantly targeting RIN4, we attempted to visualize the two proteins *in silico* via AlphaFold. The software could not predict a complex between RipE1 and RIN4 in a confident manner, thus, the results of this analysis were inconclusive (data not shown). This could be partially explained by the fact that RIN4 is considered an intrinsically disordered protein,[58] making its structural prediction very challenging with existing tools, even in complexes. However, our data already suggested that *Nb*RIN4 could be a potential target of RipE1. When we initially measured *Nb*RIN4 levels co-expressed with *Nb*Exo70B1, we detected a significant difference between the cases involving the addition of wild type RipE1, compared to that of its derived mutant C172A. Specifically, as measured by mCherry signal intensity, RipE1 significantly quenched the *Nb*RIN4-derived signal depending on the effector's protease activity (Figures 4E and 4G). Furthermore, further investigation revealed that *Nb*RIN4 interacted with RipE1 both in yeast (Figure 5A) and *in planta* (Figure 5B). In line with the previously studied corresponding proteins from Arabidopsis,[26] *Nb*RIN4 also interacted with *Nb*Exo70B1 in yeast (Figure 5A). We additionally confirmed that *Nb*Exo70B1 and *Nb*RIN4 associate with each other *in planta* (Figures 5C and S3F). In fact, when BiFC analysis was performed for these two proteins (Figure 5C), YFP signal was detected in small foci, in accordance with how the corresponding Arabidopsis proteins behaved in similar BiFC analysis (Figure S3E). These observations suggest the existence of conserved mechanisms in the two model plant systems involving the Exo70B1-RIN4 complex. To further elucidate the relationship between RipE1 and RIN4 we tested if RipE1 could promote RIN4 degradation *in planta,* without the additional over-expression of *Nb*Exo70B1. Notably, wild type RipE1 significantly lowered *Nb*RIN4 protein levels, compared to its derived mutant C172A, as revealed by immunoblotting after the transient expression of the respective proteins *in planta* (Figures 5D and 5E). Furthermore, when we monitored the levels of endogenous *Nb*RIN4 in the presence of RipE1, we observed that RIN4 seemed to be degraded after the transient expression of wild type RipE1 but not of its derived mutants RipE1(C172A) and RipE1 ΔA (Figure 5F). Based on our results so far and on the existing literature,[43] we decided to test if the decreasing of *Nb*RIN4 and *Nb*Exo70B1 levels by the cysteine protease activity of RipE1 could be linked to the recognition mechanism of this conserved *R. solanacearum* effector in *N. benthamiana*.

Nicotiana benthamiana immune receptor *Pseudomonas tomato race 1* (Ptr1) recognizes RipE1 protease activity

RipE1-induced cell death in *N. benthamiana* seems to be independent of EDS1,[43] NRG1, and ADR1 (Figures S4A and S4B). Since both EDS1 and NRG1 have been linked to signaling downstream to TIR-NLRs (TNLs) activation, it is reasonable to hypothesize that the NLR responsible for RipE1 recognition in *N. benthamiana* is a non-TIR-NLR and very likely it is a CC-NLR (CNL).[59] In addition, considering RipE1 failed to activate cell death in *N. sylvestris*, a homolog of this "suspected" NLR is likely not present in *N. sylvestris* genome, but it should be present in *N. tabacum*[42] and *N. benthamiana*. No such NLR has been associated with monitoring Exo70 proteins' integrity in tobacco plants. However, it has been previously shown that a CC-NLR with such characteristics, named *Pseudomonas* tomato race 1 (Ptr1), is present in *N. benthamiana* and has been associated with the cleavage of RIN4 by pathogen effectors.[34,35] The Arabidopsis CC-NLR, RPM1, has also been linked to the guarding of RIN4 against *P. syringae* effectors AvrB and AvrRpm1.[31] However, an RPM1 homolog was not discovered in *N. benthamiana* and *N. tabacum* genomes in our genome mining analysis and this was also the case for a third RIN4-guarding NLR, the Arabidopsis Resistance to *Pseudomonas syringae 2* (RPS2), which guards RIN4 against AvrRpt2-mediated cleavage.[32] Considering this information, along with the observed association between RipE1 and *Nb*RIN4 and the degradation of *Nb*RIN4 in the presence of RipE1 (Figure 5), we hypothesized that the most suitable candidate NLR to test for RipE1-induced cell death in *N. benthamiana* was *Nb*Ptr1. To initially test our hypothesis, we transiently co-expressed *Nb*Ptr1 with RipE1 in *N. sylvestris* leaves via *Agrobacterium*-mediated infiltration (Figure 6A). Interestingly, the ectopic expression of *Nb*Ptr1 in *N. sylvestris* did not activate cell death when it was expressed without RIN4. Furthermore, the co-expression of *Nb*Ptr1 with the wild type RipE1 in *N. sylvestris* activated a strong cell death phenotype, while such a phenotype was not observed when the inactive mutated RipE1-C172A was co-expressed with *Nb*Ptr1 (Figure 6A). These results indicate that *Nb*Ptr1 mediates the recognition of RipE1, dependent on the effector's cysteine protease activity, when ectopically expressed in *N. sylvestris*. To confirm *Nb*Ptr1 requirement for RipE1 recognition in *N. benthamiana*, we used an *Agrobacterium*-mediated hairpin-based silencing system[60] to transiently silence *Nb*Ptr1 gene expression (Figure 6B). RipE1 expression failed to activate cell

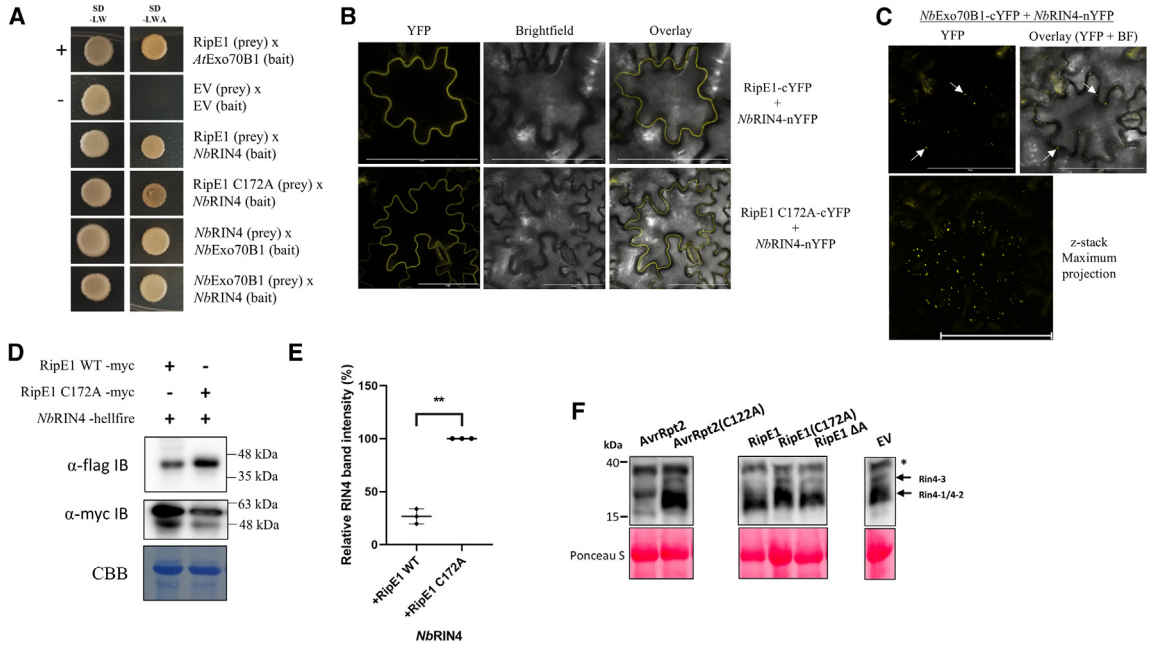

Figure 5. RipE1 targets *Nicotiana benthamiana* RIN4 via its cysteine protease activity

(A) Yeast two-hybrid assays to test the interaction between RipE1 and its derived mutant RipE1 C172A and *Nicotiana benthamiana* protein RIN4. Interaction between the *N. benthamiana* proteins Exo70B1 and RIN4 was also tested. Interaction between RipE1 and *At*Exo70B1 was used as a positive control. Yeast cells carrying the indicated baits and preys were spotted on SDC-LW and SDC-LWA selective plates. Photographs were taken after 4 days of incubation.

(B) *In planta* association of RipE1 and its derived mutant RipE1 C172A with *Nicotiana benthamiana* protein RIN4. Proteins of interest were fused at their C-termini with cCFP (cYFP) or nVenus (nYFP) epitope tags, as indicated, and the YFP signal was detected via confocal microscopy 48 hpi. Scale bars are 70 μm.

(C) *In planta* association between *Nicotiana benthamiana* proteins Exo70B1 and RIN4. Proteins of interest were fused at their C-termini with cCFP (cYFP) or nVenus (nYFP) epitope tags, as indicated, and the YFP signal was detected via confocal microscopy 48 hpi. YFP signal was detected in small foci around the cell, as indicated by white arrows and as highlighted by the z stack maximum projection image. Scale bars are 70 μm. A similar assay using the corresponding proteins in Arabidopsis is presented in Figure S3E.

(D) Representative immunoblots used for the statistical analysis in Figure 5E. *Nicotiana benthamiana* RIN4 C-terminally fused to the hellfire tag (6xHis-3xFLAG) was transiently co-expressed in *N. sylvestris* leaves with wild type RipE1 or its derived mutant C172A, C-terminally fused to the myc tag. Proteins were extracted at 3 dpi. Expected protein sizes: *Nb*RIN4-hellfire at 77 kDa and RipE1 WT or RipE1 C172A-myc at 52 kDa.

(E) Statistical analysis to examine the possible RipE1-promoted degradation of *N. benthamiana* RIN4, after their transient co-expression. Relative *Nb*RIN4 band intensity in immunoblot analysis was measured via FiJi in the immunoblots from 3 biological replicates. *Nb*RIN4 protein levels in the presence of wild type RipE1 were compared to those in the presence of mutated RipE1 C172A as a means to detect any possible *Nb*RIN4 degradation caused by the catalytic activity of RipE1. For the statistical analysis, *Nb*RIN4 relative band intensity measurements from all 3 biological replicates were submitted to t-test followed by Welch's correction. $^{**}p$ value = 0.003.

(F) RipE1 causes the degradation of endogenous *N. benthamiana* RIN4 *in planta*. Genes of interest (effectors or EV) were transiently expressed in *N. benthamiana* leaves via *Agrobacterium*-mediated infiltration. Leaf disc samples from infiltrated areas were taken 46 hpi and RIN4 expression was measured via immunoblotting using an anti-RIN4 antibody. RIN4-3 appeared to be degraded in the presence of wild type RipE1 but not its derived mutants RipE1 (C172A) and RipE1 ΔA. Wild type AvrRpt2 was used as a positive RIN4-degrading control, while AvrRpt2 (C122A) mutant and EV served as negative controls. Asterisk indicates an unknown cross-reacting protein.

death when transiently expressed in an *N. benthamiana* leaf area priorly infiltrated with an *Nb*Ptr1-targeting silencing hairpin (hp) construct (Figure 6B). In addition, we performed cell death assays by transiently expressing RipE1 in *N. benthamiana ptr1* knock-out plants (Nb1-ptr1).[61] RipE1 transient expression failed to induce cell death in Nb1-ptr1 plants (Figure 6C), while the transient co-expression of *Nb*Ptr1 and RipE1 in these plants was able to complement the activation of cell death (Figure 6D). Overall, these observations, along with some recent independently produced yet similar findings,[55] suggest that *N. benthamiana* CC-NLR *Nb*Ptr1 is required for the activation of cell death by RipE1.

The evidence presented in this work supports the hypothesis that RipE1 targets the plant cell's membrane trafficking components Exo70B1 and RIN4, possibly adding the manipulation of the host secretion machinery by RipE1 to the pathogen's large arsenal of virulence factors. Membrane trafficking appears to be a major target of not only plant pathogenic microorganisms but also some studied examples of mammal pathogens.[17,62,63] While most reports of membrane trafficking manipulation by plant pathogen effectors refer to suppressing defense-related secretion,[62] persistent intracellular mammal pathogens, such as *Salmonella*, utilize effectors to exploit the host's secretion machinery, promoting both their internalization and their spread.[64,65] Notably, the discoveries of this study were initially derived from a Y2H screening against a collection of NLR-IDs. Further investigation of the interaction between RipE1 and an NLR-ID ultimately resulted in granting novel insight to the activity

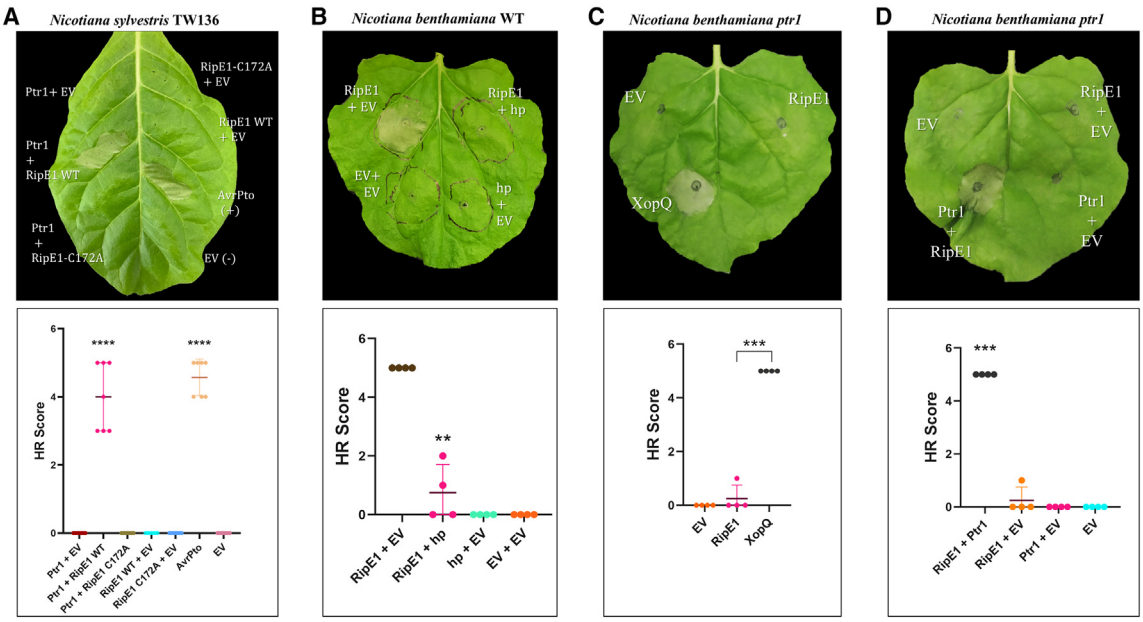

Figure 6. *Nicotiana benthamiana* immune receptor *Pseudomonas tomato race 1* (Ptr1) recognizes RipE1 protease activity

(A) RipE1 activity ectopically induces *Nb*Ptr1-dependent cell death. The *N. sylvestris* leaf in the top panel represents one of the 7 biological replicates used for the statistical analysis of hypersensitive response (HR) assays presented in the bottom panel. The indicated proteins were transiently expressed via *Agrobacterium*-mediated infiltration at a total OD_{600} of 0.5. AvrPto transient expression was used as an HR-activating positive control in *N. sylvestris*. Empty vector (EV) was used as a negative control and also to balance total co-infiltrations inoculum OD_{600}. The photograph presented here was captured at 3 dpi. To quantify the results of these experiments, HR scores representing cell death severity were first assigned to the observed phenotypes from 7 biological replicates. For the statistical analysis, assigned HR scores from all 7 replicates were then submitted to t-test followed by Welch's correction. ****p value < 0.0001.

(B) Silencing of *Nb*Ptr1 abolishes RipE1-induced cell death in *N. benthamiana*. This experiment was performed according to Brendolise et al., where agro-infiltrations are performed on two subsequent days. On the first day, the two right patches were infiltrated with agrobacteria carrying the hairpin construct (hp), while the two left patches were infiltrated with agrobacteria carrying the corresponding empty vector (EV). The following day, the two upper patches were infiltrated with agrobacteria carrying a RipE1 construct, while the two bottom patches were infiltrated with agrobacteria carrying the corresponding empty vector. Photographs were taken 3 days after RipE1 infiltration. The photograph in the top panel represents one of the 4 biological replicates used for the statistical analysis of hypersensitive response (HR) assays presented in the bottom panel. To quantify the results of these experiments, HR scores representing cell death severity were first assigned to the observed phenotypes from 4 biological replicates. For the statistical analysis, assigned HR scores from all 4 replicates were then submitted to a t-test followed by Welch's correction. **p value = 0.003.

(C) RipE1 does not activate cell death in *N. benthamiana* ptr1 mutant plants. *Xcv*XopQ was used as an HR-inducing positive control. Indicated proteins were transiently expressed via *Agrobacterium*-mediated infiltration at a total OD_{600} of 0.2. The photograph in the top panel was captured at 4 dpi and represents one of the 4 biological replicates used for the statistical analysis of hypersensitive response (HR) assays presented in the bottom panel. To quantify the results of these experiments, HR scores representing cell death severity were first assigned to the observed phenotypes from 4 biological replicates. For the statistical analysis, assigned HR scores from all 4 replicates were then submitted to a t-test followed by Welch's correction. ***p value = 0.0003.

(D) RipE1 and Ptr1 co-expression rescues cell death activation in *N. benthamiana* ptr1 mutant plants. Indicated proteins were transiently expressed via *Agrobacterium*-mediated infiltration at a total OD_{600} of 0.2. The photograph in the top panel was captured at 4 dpi and represents one of the 4 biological replicates used for the statistical analysis of hypersensitive response (HR) assays presented in the bottom panel. To quantify the results of these experiments, HR scores representing cell death severity were first assigned to the observed phenotypes from 4 biological replicates. For the statistical analysis, assigned HR scores from all 4 replicates were then submitted to a t-test followed by Welch's correction. ***p value = 0.0003.

and recognition of RipE1. The strategy used here highlights the benefits of employing NLR-ID domains as the means to uncover new potential targets and functions of pathogen effectors.

Overall, the data presented and discussed here, along with the existing literature, collectively point to a working model possibly connecting RipE1 targeting of membrane trafficking components to the molecular mechanism underlying its recognition in *N. benthamiana* (Figure 7). In our efforts to uncover putative RipE1 subcellular targets, we observed that RipE1 can cause not only RIN4 degradation but also Exo70B1 degradation when RIN4 is present. Given the known relationship between the two plant proteins,[26,28–30] one plausible interpretation of these results is that RipE1 may indirectly compromise Exo70B1 via targeting RIN4. In addition, based on earlier evidence heavily pointing to *Nb*Ptr1 being an RIN4-guarding NLR,[34,35] we also observed the ability of *Nb*Ptr1 to recognize RipE1 activity. Interestingly, while RPM1 ectopic overexpression in tobacco results in cell death unless RIN4 is also over-expressed,[66,67] *Nb*Ptr1 ectopic over-expression in *N. sylvestris* did not elicit cell death in our experimental conditions. Considering this, *Nb*Ptr1 may monitor RIN4 without a physical association with it, leaving open the possibility that other RIN4-interacting proteins -like Exo70B1- are implicated in this process. Although further research is required to probe the functional importance of RipE1 activity upon Exo70B1 and RIN4, our working model suggests the possibility of RipE1 detection by *Nb*Ptr1

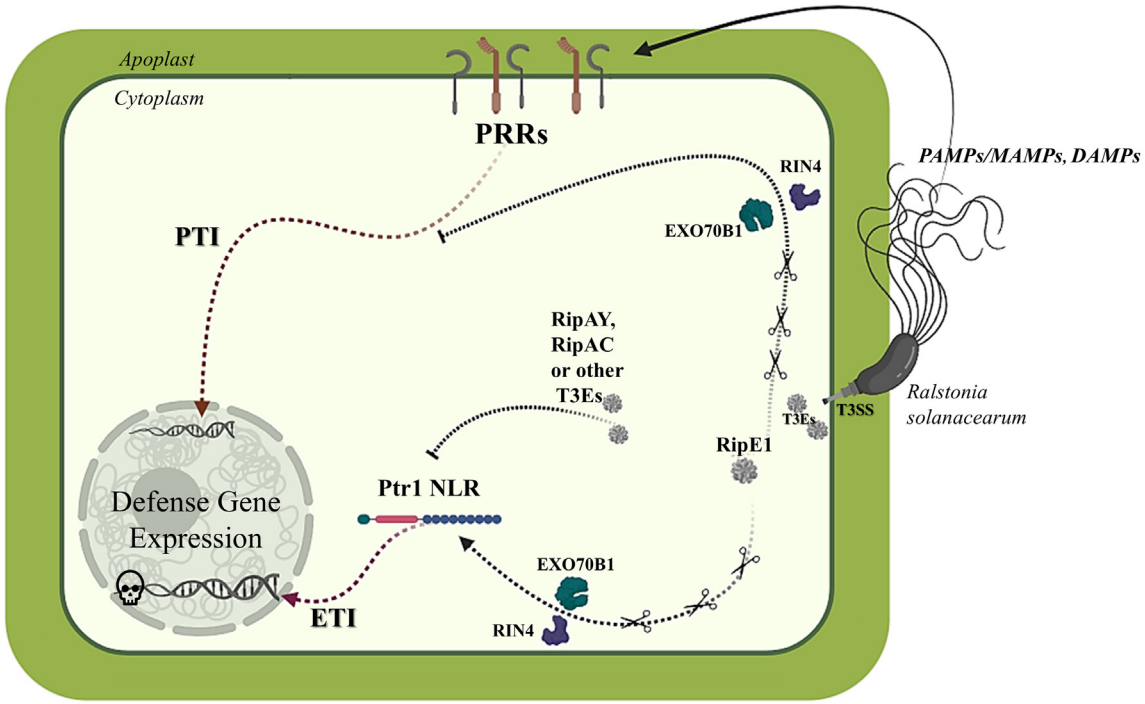

Figure 7. Proposed model describing the molecular mechanism of RipE1 activity and its recognition

Upon *Ralstonia solanacearum* infection, RipE1 is delivered into the cytoplasm among other numerous effectors. RipE1 associates with both Exo70B1 and RIN4 at the PM, where the two of them interact. Proteolytic cleavage of either Exo70B1 or RIN4 (or both) by RipE1 could aim to suppress immunity-related responses mediated by these two proteins but at the same time could be linked to the activation of Ptr1-induced cell death. RipE1 cysteine protease activity is perceived by Ptr1, activating cell death. Other T3Es secreted by *R. solanacearum*, such as RipAC[44] or RipAY[43] can potentially suppress RipE1-triggered cell death, allowing the effector to attain its potential immunity-suppressing properties.

being due to the compromising of either Exo70B1 or RIN4 or both. Nevertheless, further investigation is required in order to decipher the complete pathway of cell death activation by *Nb*Ptr1 after the RipE1-induced degradation of RIN4 and to determine if Exo70B1 or other RIN4-interacting proteins are involved in this mechanism.

Limitations of the study

Our study focused on uncovering subcellular targets of *Ralstonia solanacearum* type III effector RipE1 and their possible involvement in the effector's recognition mechanism. However, as discussed earlier, RipE1 appears to have multiple potential subcellular targets. Therefore, in order to have a more complete picture regarding RipE1 functions inside the host cell, its whole interactome needs to be further investigated. In addition, here we reported *N. sylvestris* as a potent model to study RipE1 in planta, yet the lack of availability of a completely annotated and high-quality *N. sylvestris* genome in the designated databases has limited the possible tools and resources we could develop for this model.

RESOURCE AVAILABILITY

Lead contact

Further information and requests for resources and reagents should be directed to and will be fulfilled by the lead contact, Panagiotis F. Sarris (p.sarris@imbb.forth.gr).

Materials availability

All unique materials used in this study will be available upon request.

Data and code availability

The mass spectrometry proteomics data have been deposited to the ProteomeXchange Consortium via the PRIDE[68] partner repository with the dataset identifier PXD041406.

ACKNOWLEDGMENTS

The authors thank Prof. Nemo Peeters for his kind donation of the *R. solanacearum* GMI1000 strain and Prof. Dimitris Goumas for his guidance with culturing and handling the bacteria; Dr. Matthew Moscou for the kind donation of some of the IDs used in this study; Prof. Despina Alexandraki for her generous donation of the yeast strain PJ69; Mr Marc Youles and the Synthetic Biology Group of TSL for their kind donation of Golden-Gate-Cloning compatible vectors for Y2H assays; Mrs Dina Kotsifaki for her valuable help during protein purification; Dr. Patrick Celie for his kind donation of the LIC 1.10 vector; Dr. Cyril Brendolise for his generous donation of the *Nb*Ptr1 hairpin construct; Prof. Gitta Coaker for her generous donation of α-RIN4 antibody and lastly postdoctoral fellow Dr Glykeria Mermigka for her advice and fruitful discussion throughout the experiments.

D.T. was supported by the Hellenic Foundation for Research and Innovation (HFRI) and the General Secretariat for Research and Technology (GSRT), under the HFRI PhD Fellowship grant (GA. no. 11075). K.K. was supported by iNEXT-Discovery, project number 871037, funded by the Horizon 2020 program of the European Commission. NZ and GBM were supported by US National Science Foundation grant IOS-1546625 and the Triad Foundation. The funders had no role in study design, data collection and analysis, the decision to publish, or preparation of the article.

AUTHOR CONTRIBUTIONS

P.F.S. designed the research and supervised the project; D.T. carried out the experiments; K.K. purified recombinant proteins and performed *in vitro* protein assays and performed the AlphaFold analysis; V.A.M. supervised the confocal microscopy experiments and contributed to *Nb*Ptr1 cloning for transient expression; S.M. contributed to silencing assays; N.K. performed the MS/MS analysis; M.K. and V.A.M., contributed experimental materials; NZ and GBM developed the Nb1-ptr1 line, helped with the proof reading of the article and performed the RIN4 degradation assays; P.F.S., D.T., and K.K. wrote the article; P.F.S. edited the article; All authors have read and approved the article.

DECLARATION OF INTERESTS

The authors declare no competing interests.

STAR★METHODS

Detailed methods are provided in the online version of this paper and include the following:

- KEY RESOURCES TABLE
- METHOD DETAILS
  - *In silico* protein structure prediction and analysis
  - Plasmid construction
  - Bacterial strains and growth conditions
  - Y2H assay
  - Plant material
  - Generation of *Nicotiana benthamiana ptr1* mutant lines using CRISPR/Cas9
  - Confocal microscopy
  - Protein extraction from plant leaf tissue
  - Protein extraction from yeast cells
  - Co-immunoprecipitation
  - PM/cell fractionation from plant tissue
  - SDS PAGE and immunoblotting
  - Protein production and purification
  - *In vitro* cleavage assay
  - NanoLC-MS/MS analysis
  - Data analysis of MS/MS-derived data
  - Statistical analysis and plotting of hypersensitive response (HR) assay results
  - RIN4 degradation assay
  - *Agrobacterium*-mediated hairpin-based silencing

SUPPLEMENTAL INFORMATION

Supplemental information can be found online at https://doi.org/10.1016/j.isci.2025.112307.

Received: February 12, 2024
Revised: May 23, 2024
Accepted: March 10, 2025
Published: March 28, 2025

REFERENCES

1. Duxbury, Z., Ma, Y., Furzer, O.J., Huh, S.U., Cevik, V., Jones, J.D.G., and Sarris, P.F. (2016). Pathogen perception by NLRs in plants and animals: Parallel worlds. Bioessays *38*, 769–781. https://doi.org/10.1002/bies.201600046.
2. Mermigka, G., Amprazi, M., Mentzelopoulou, A., Amartolou, A., and Sarris, P.F. (2020). Plant and Animal Innate Immunity Complexes: Fighting Different Enemies with Similar Weapons. Trends Plant Sci. *25*, 80–91. https://doi.org/10.1016/j.tplants.2019.09.008.
3. Lal, N.K., Thanasuwat, B., Huang, P.J., Cavanaugh, K.A., Carter, A., Michelmore, R.W., and Dinesh-Kumar, S.P. (2020). Phytopathogen Effectors Use Multiple Mechanisms to Manipulate Plant Autophagy. Cell Host Microbe *28*, 558–571.e6. https://doi.org/10.1016/j.chom.2020.07.010.
4. Khan, M., Seto, D., Subramaniam, R., and Desveaux, D. (2018). Oh, the places they'll go! A survey of phytopathogen effectors and their host targets. Plant J. *93*, 651–663. https://doi.org/10.1111/tpj.13780.
5. Schreiber, K.J., Chau-Ly, I.J., and Lewis, J.D. (2021). What the wild things do: Mechanisms of plant host manipulation by bacterial type III-secreted effector proteins. Microorganisms *9*, 1029. https://doi.org/10.3390/microorganisms9051029.
6. Yuan, M., Jiang, Z., Bi, G., Nomura, K., Liu, M., He, S.Y., Zhou, J.M., and Xin, X.F. (2021). Pattern-recognition receptors are required for NLR-mediated plant immunity. Nature *592*, 105–109. https://doi.org/10.1101/2020.04.10.031294.
7. Yuan, M., Ngou, B.P.M., Ding, P., and Xin, X.F. (2021). PTI-ETI crosstalk: an integrative view of plant immunity. Curr. Opin. Plant Biol. *62*, 102030. https://doi.org/10.1016/j.pbi.2021.102030.
8. Jones, J.D.G., and Dangl, J.L. (2006). The plant immune system. Nature *444*, 323–329.
9. Kapos, P., Devendrakumar, K.T., and Li, X. (2019). Plant NLRs: From discovery to application. Plant Sci. *279*, 3–18. https://doi.org/10.1016/j.plantsci.2018.03.010.
10. Li, X., Kapos, P., and Zhang, Y. (2015). NLRs in plants. Curr. Opin. Immunol. *32*, 114–121. https://doi.org/10.1016/j.coi.2015.01.014.
11. Camagna, M., and Takemoto, D. (2018). Hypersensitive Response in Plants. eLS, 1–7, John Wiley & Sons, Ltd (Ed.). https://doi.org/10.1002/9780470015902.a0020103.pub2.
12. Cesari, S. (2018). Multiple strategies for pathogen perception by plant immune receptors. New Phytol. *219*, 17–24. https://doi.org/10.1111/nph.14877.
13. van der Hoorn, R.A.L., and Kamoun, S. (2008). From Guard to Decoy: A New Model for Perception of Plant Pathogen Effectors. Plant Cell *20*, 2009–2017. https://doi.org/10.1105/tpc.108.060194.
14. Sarris, P.F., Cevik, V., Dagdas, G., Jones, J.D.G., and Krasileva, K.V. (2016). Comparative analysis of plant immune receptor architectures uncovers host proteins likely targeted by pathogens. BMC Biol. *14*, 8. https://doi.org/10.1186/s12915-016-0228-7.
15. Baggs, E., Dagdas, G., and Krasileva, K.V. (2017). NLR diversity, helpers and integrated domains: making sense of the NLR IDentity. Curr. Opin. Plant Biol. *38*, 59–67. https://doi.org/10.1016/j.pbi.2017.04.012.
16. Marchal, C., Michalopoulou, V.A., Zou, Z., Cevik, V., and Sarris, P.F. (2022). Show me your ID : NLR immune receptors with integrated domains in plants. Essays Biochem. *66*, 527–539. https://doi.org/10.1042/EBC20210084.
17. Gu, Y., Zavaliev, R., and Dong, X. (2017). Membrane Trafficking in Plant Immunity. Mol. Plant *10*, 1026–1034. https://doi.org/10.1016/j.molp.2017.07.001.
18. Saeed, B., Brillada, C., and Trujillo, M. (2019). Dissecting the plant exocyst. Curr. Opin. Plant Biol. *52*, 69–76. https://doi.org/10.1016/j.pbi.2019.08.004.
19. Mei, K., and Guo, W. (2018). The exocyst complex. Curr. Biol. *28*, R922–R925. https://doi.org/10.1016/j.cub.2018.06.042.
20. Picco, A., Irastorza-Azcarate, I., Specht, T., Böke, D., Pazos, I., Rivier-Cordey, A.S., Devos, D.P., Kaksonen, M., and Gallego, O. (2017). The In Vivo Architecture of the Exocyst Provides Structural Basis for Exocytosis. Cell *168*, 400–412.e18. https://doi.org/10.1016/j.cell.2017.01.004.
21. Elias, M., Drdova, E., Ziak, D., Bavlnka, B., Hala, M., Cvrckova, F., Soukupova, H., and Zarsky, V. (2003). The exocyst complex in plants. Cell. Biol. Int. *27*, 199–201. https://doi.org/10.1016/S1065-6995(02)00349-9.
22. Du, Y., Overdijk, E.J.R., Berg, J.A., Govers, F., and Bouwmeester, K. (2018). Solanaceous exocyst subunits are involved in immunity to diverse

plant pathogens. J. Exp. Bot. *69*, 655–666. https://doi.org/10.1093/jxb/erx442.

23. Wang, W., Liu, N., Gao, C., Rui, L., and Tang, D. (2019). The Pseudomonas Syringae Effector AvrPtoB Associates With and Ubiquitinates Arabidopsis Exocyst Subunit EXO70B1. Front. Plant Sci. *10*, 1027. https://doi.org/10.3389/fpls.2019.01027.
24. Michalopoulou, V.A., Mermigka, G., Kotsaridis, K., Mentzelopoulou, A., Celie, P.H.N., Moschou, P.N., Jones, J.D.G., and Sarris, P.F. (2022). The host exocyst complex is targeted by a conserved bacterial type III effector protein that promotes virulence. Plant Cell *34*, 3400–3424. https://doi.org/10.1093/plcell/koac162.
25. Afzal, A.J., da Cunha, L., and Mackey, D. (2011). Separable fragments and membrane tethering of Arabidopsis RIN4 regulate its suppression of PAMP-triggered immunity. Plant Cell *23*, 3798–3811. https://doi.org/10.1105/tpc.111.088708.
26. Sabol, P., Kulich, I., and Žárský, V. (2017). RIN4 recruits the exocyst subunit EXO70B1 to the plasma membrane. J. Exp. Bot. *68*, 3253–3265. https://doi.org/10.1093/jxb/erx007.
27. Zhao, T., Rui, L., Li, J., Nishimura, M.T., Vogel, J.P., Liu, N., Liu, S., Zhao, Y., Dangl, J.L., and Tang, D. (2015). A Truncated NLR Protein, TIR-NBS2, Is Required for Activated Defense Responses in the exo70B1 Mutant. PLoS Genet. *11*, e1004945. https://doi.org/10.1371/journal.pgen.1004945.
28. Redditt, T.J., Chung, E.-H., Zand Karimi, H., Rodibaugh, N., Zhang, Y., Trinidad, J.C., Kim, J.H., Zhou, Q., Shen, M., Dangl, J.L., et al. (2019). AvrRpm1 Functions as an ADP-Ribosyl Transferase to Modify NOI-domain Containing Proteins, Including Arabidopsis and Soybean RPM1-interacting Protein 4. Plant Cell *31*, 00020. https://doi.org/10.1105/tpc.19.00020.
29. Wu, X., Huang, J., Cao, Y., and Gao, Z. (2021). The resistance associated protein RIN4 promotes the extracellular transport of AtEXO70E2. Biochem. Biophys. Res. Commun. *555*, 40–45. https://doi.org/10.1016/j.bbrc.2021.03.072.
30. Fujisaki, K., Abe, Y., Kanzaki, E., Ito, K., Utsushi, H., Saitoh, H., Białas, A., Banfield, M.J., Kamoun, S., and Terauchi, R. (2017). An unconventional NOI/RIN4 domain of a rice NLR protein binds host EXO70 protein to confer fungal immunity. Preprint at bioRxiv, 1–14. https://doi.org/10.1101/239400.
31. Mackey, D., Holt, B.F., Wiig, A., and Dangl, J.L. (2002). RIN4 interacts with Pseudomonas syringae type III effector molecules and is required for RPM1-mediated resistance in Arabidopsis. Cell *108*, 743–754. https://doi.org/10.1016/S0092-8674(02)00661-X.
32. Mackey, D., Belkhadir, Y., Alonso, J.M., Ecker, J.R., and Dangl, J.L. (2003). Arabidopsis RIN4 is a target of the type III virulence effector AvrRpt2 and modulates RPS2-mediated resistance. Cell *112*, 379–389. https://doi.org/10.1016/S0092-8674(03)00040-0.
33. Liu, J., Elmore, J.M., Lin, Z.J.D., and Coaker, G. (2011). A receptor-like cytoplasmic kinase phosphorylates the host target RIN4, leading to the activation of a plant innate immune receptor. Cell Host Microbe *9*, 137–146. https://doi.org/10.1016/j.chom.2011.01.010.
34. Mazo-Molina, C., Mainiero, S., Hind, S.R., Kraus, C.M., Vachev, M., Maviane-Macia, F., Lindeberg, M., Saha, S., Strickler, S.R., Feder, A., et al. (2019). The ptr1 locus of solanum lycopersicoides confers resistance to race 1 strains of pseudomonas syringae pv. tomato and to ralstonia pseudosolanacearum by recognizing the type III effectors AvrRpt2 and RipBN. Mol. Plant Microbe Interact. *32*, 949–960. https://doi.org/10.1094/MPMI-01-19-0018-R.
35. Mazo-Molina, C., Mainiero, S., Haefner, B.J., Bednarek, R., Zhang, J., Feder, A., Shi, K., Strickler, S.R., and Martin, G.B. (2020). Ptr1 evolved convergently with RPS2 and Mr5 to mediate recognition of AvrRpt2 in diverse solanaceous species. Plant J. *103*, 1433–1445. https://doi.org/10.1111/tpj.14810.
36. Luo, Y., Caldwell, K.S., Wroblewski, T., Wright, M.E., and Michelmore, R.W. (2009). Proteolysis of a negative regulator of innate immunity is dependent on resistance genes in tomato and nicotiana benthamiana and induced by multiple bacterial effectors. Plant Cell *21*, 2458–2472. https://doi.org/10.1105/tpc.107.056044.
37. Landry, D., González-Fuente, M., Deslandes, L., and Peeters, N. (2020). The large, diverse, and robust arsenal of Ralstonia solanacearum type III effectors and their in planta functions. Mol. Plant Pathol. *21*, 1377–1388. https://doi.org/10.1111/mpp.12977.
38. Mansfield, J., Genin, S., Magori, S., Citovsky, V., Sriariyanum, M., Ronald, P., Dow, M., Verdier, V., Beer, S.V., Machado, M.A., et al. (2012). Top 10 plant pathogenic bacteria in molecular plant pathology. Mol. Plant Pathol. *13*, 614–629. https://doi.org/10.1111/j.1364-3703.2012.00804.x.
39. Sabbagh, C.R.R., Carrere, S., Lonjon, F., Vailleau, F., Macho, A.P., Genin, S., and Peeters, N. (2019). Pangenomic type III effector database of the plant pathogenic Ralstonia spp. PeerJ *7*, e7346. https://doi.org/10.7717/peerj.7346.
40. Peeters, N., Carrère, S., Anisimova, M., Plener, L., Cazalé, A.-C., and Genin, S. (2013). Repertoire, unified nomenclature and evolution of the Type III effector gene set in the Ralstonia solanacearum species complex. BMC. Genomics. *14*, 859. https://doi.org/10.1186/1471-2164-14-859.
41. Nakano, M., and Mukaihara, T. (2019). Comprehensive Identification of PTI Suppressors in Type III Effector Repertoire Reveals that Ralstonia solanacearum Activates Jasmonate Signaling at Two Different Steps. Int. J. Mol. Sci. *20*, 5992.
42. Jeon, H., Kim, W., Kim, B., Lee, S., Jayaraman, J., Jung, G., Choi, S., Sohn, K.H., and Segonzac, C. (2020). Ralstonia solanacearum type III effectors with predicted nuclear localization signal localize to various cell compartments and modulate immune responses in nicotiana spp. Plant Pathol. J. *36*, 43–53. https://doi.org/10.5423/PPJ.OA.08.2019.0227.
43. Sang, Y., Yu, W., Zhuang, H., Wei, Y., Derevnina, L., Yu, G., Luo, J., and Macho, A.P. (2020). Intra-strain Elicitation and Suppression of Plant Immunity by Ralstonia solanacearum Type-III Effectors in Nicotiana benthamiana. Plant Commun. *1*, 100025. https://doi.org/10.1016/j.xplc.2020.100025.
44. Yu, G., Xian, L., Xue, H., Yu, W., Rufian, J.S., Sang, Y., Morcillo, R.J.L., Wang, Y., and Macho, A.P. (2020). A bacterial effector protein prevents mapk-mediated phosphorylation of sgt1 to suppress plant immunity. PLoS Pathog. *16*, e1008933. https://doi.org/10.1371/journal.ppat.1008933.
45. Nakano, M., Ichinose, Y., and Mukaihara, T. (2021). Ralstonia solanacearum Type III Effector RipAC Targets SGT1 to Suppress Effector-Triggered Immunity. Plant Cell Physiol. *61*, 2067–2076. https://doi.org/10.1093/pcp/pcaa122.
46. Fowler, N.J., and Williamson, M.P. (2022). The accuracy of protein structures in solution determined by AlphaFold and NMR. Structure *30*, 925–933.e2. https://doi.org/10.1016/j.str.2022.04.005.
47. Kotsaridis, K., Michalopoulou, V.A., Tsakiri, D., Kotsifaki, D., Kefala, A., Kountourakis, N., Celie, P.H.N., Kokkinidis, M., and Sarris, P.F. (2023). The functional and structural characterization of Xanthomonas campestris pv. campestris core effector XopP revealed a new kinase activity. Plant J. *116*, 100–111. https://doi.org/10.1111/tpj.16362.
48. Rawat, A., Roy, M., Jyoti, A., Kaushik, S., Verma, K., and Srivastava, V.K. (2021). Cysteine proteases: Battling pathogenic parasitic protozoans with omnipresent enzymes. Microbiol. Res. *249*, 126784. https://doi.org/10.1016/j.micres.2021.126784.
49. Holm, L. (2020). Using Dali for Protein Structure Comparison. Methods. Mol. Biol. *2112*, 29–42. https://doi.org/10.1007/978-1-0716-0270-6_3.
50. Chatterjee, D., Boyd, C.D., O'Toole, G.A., and Sondermann, H. (2012). Structural characterization of a conserved, calcium-dependent periplasmic protease from Legionella pneumophila. J. Bacteriol. *194*, 4415–4425. https://doi.org/10.1128/JB.00640-12.
51. Nimchuk, Z.L., Fisher, E.J., Desveaux, D., Chang, J.H., and Dangl, J.L. (2007). The HopX (AvrPphE) Family of Pseudomonas syringae Type III Effectors Require a Catalytic Triad and a Novel N-Terminal Domain for

Function. Mol. Plant Microbe Interact. *20*, 346–357. https://doi.org/10.1094/mpmi-20-4-0346.

52. Gimenez-Ibanez, S., Boter, M., Fernández-Barbero, G., Chini, A., Rathjen, J.P., and Solano, R. (2014). The Bacterial Effector HopX1 Targets JAZ Transcriptional Repressors to Activate Jasmonate Signaling and Promote Infection in Arabidopsis. PLoS Biol. *12*, 1001792. https://doi.org/10.1371/journal.pbio.1001792.

53. Kotsaridis, K., Tsakiri, D., and Sarris, P.F. (2023). Understanding enemy's weapons to an effective prevention: common virulence effects across microbial phytopathogens kingdoms. Crit. Rev. Microbiol. *49*, 528–542. https://doi.org/10.1080/1040841X.2022.2083939.

54. Covarrubias, A.A., Romero-Pérez, P.S., Cuevas-Velazquez, C.L., and Rendón-Luna, D.F. (2020). The functional diversity of structural disorder in plant proteins. Arch. Biochem. Biophys. *680*, 108229. https://doi.org/10.1016/j.abb.2019.108229.

55. Kim, B., Kim, I., Yu, W., Li, M., Kim, H., Ahn, Y.J., Sohn, K.H., Macho, A.P., and Segonzac, C. (2023). The Ralstonia pseudosolanacearum effector RipE1 is recognized at the plasma membrane by NbPtr1, the Nicotiana benthamiana homologue of Pseudomonas tomato race 1. Mol. Plant Pathol. *24*, 1312–1318. https://doi.org/10.1111/mpp.13363.

56. Liu, N., Hake, K., Wang, W., Zhao, T., Romeis, T., and Tang, D. (2017). Calcium-dependent protein kinase5 associates with the truncated NLR protein TIR-NBS2 to contribute to exo70B1-mediated immunity. Plant. Cell. *29*, 746–759. https://doi.org/10.1105/tpc.16.00822.

57. Zhao, G., Guo, D., Wang, L., Li, H., Wang, C., and Guo, X. (2021). Functions of RPM1-interacting protein 4 in plant immunity. Planta *253*, 11. https://doi.org/10.1007/s00425-020-03527-7.

58. Lee, D., Bourdais, G., Yu, G., Robatzek, S., and Coaker, G. (2015). Phosphorylation of the plant immune regulator RPM1-INTERACTING PROTEIN4 enhances plant plasma membrane h+-ATPase activity and inhibits flagellin-triggered immune responses in arabidopsis. Plant Cell *27*, 2042–2056. https://doi.org/10.1105/tpc.114.132308.

59. Qi, T., Seong, K., Thomazella, D.P.T., Kim, J.R., Pham, J., Seo, E., Cho, M.J., Schultink, A., and Staskawicz, B.J. (2018). NRG1 functions downstream of EDS1 to regulate TIR-NLR-mediated plant immunity in Nicotiana benthamiana. Proc. Natl. Acad. Sci. USA *115*, E10979–E10987. https://doi.org/10.1073/pnas.1814856115.

60. Brendolise, C., Montefiori, M., Dinis, R., Peeters, N., Storey, R.D., and Rikkerink, E.H. (2017). A novel hairpin library-based approach to identify NBS-LRR genes required for effector-triggered hypersensitive response in Nicotiana benthamiana. Plant Methods *13*, 32. https://doi.org/10.1186/s13007-017-0181-7.

61. Ahn, Y.J., Kim, H., Choi, S., Mazo-Molina, C., Prokchorchik, M., Zhang, N., Kim, B., Mang, H., Koehler, N., Kim, J., et al. (2023). Ptr1 and ZAR1 immune receptors confer overlapping and distinct bacterial pathogen effector specificities. New Phytol. *239*, 1935–1953. https://doi.org/10.1111/nph.19073.

62. Yuen, E.L.H., Shepherd, S., Bozkurt, T.O., and Bozkurt, T.O. (2023). Traffic Control: Subversion of Plant Membrane Trafficking by Pathogens. Annu. Rev. Phytopathol. *61*, 325–350.

63. Ireton, K., Van Ngo, H., and Bhalla, M. (2018). Interaction of microbial pathogens with host exocytic pathways. Cell. Microbiol. *20*, e12861. https://doi.org/10.1111/cmi.12861.

64. Thakur, A., Mikkelsen, H., and Jungersen, G. (2019). Intracellular pathogens: Host immunity and microbial persistence strategies. J. Immunol. Res. *2019*, 1356540. https://doi.org/10.1155/2019/1356540.

65. Hume, P.J., Singh, V., Davidson, A.C., and Koronakis, V. (2017). Swiss army pathogen: The Salmonella entry toolkit. Front. Cell. Infect. Microbiol. *7*, 348. https://doi.org/10.3389/fcimb.2017.00348.

66. Yoon, M., and Rikkerink, E.H.A. (2020). Rpa1 mediates an immune response to avrRpm1Psa and confers resistance against Pseudomonas syringae pv. Plant J. *102*, 688–702. https://doi.org/10.1111/tpj.14654.

67. Prokchorchik, M., Choi, S., Chung, E.H., Won, K., Dangl, J.L., and Sohn, K.H. (2020). A host target of a bacterial cysteine protease virulence effector plays a key role in convergent evolution of plant innate immune system receptors. New Phytol. *225*, 1327–1342. https://doi.org/10.1111/nph.16218.

68. Perez-Riverol, Y., Bai, J., Bandla, C., García-Seisdedos, D., Hewapathirana, S., Kamatchinathan, S., Kundu, D.J., Prakash, A., Frericks-Zipper, A., Eisenacher, M., et al. (2022). The PRIDE database resources in 2022: A hub for mass spectrometry-based proteomics evidences. Nucleic Acids Res. *50*, D543–D552. https://doi.org/10.1093/nar/gkab1038.

69. Zhang, Y., Chen, M., Siemiatkowska, B., Toleco, M.R., Jing, Y., Strotmann, V., Zhang, J., Stahl, Y., and Fernie, A.R. (2020). A Highly Efficient Agrobacterium-Mediated Method for Transient Gene Expression and Functional Studies in Multiple Plant Species. Plant Commun. *1*, 100028. https://doi.org/10.1016/j.xplc.2020.100028.

70. Varadi, M., Anyango, S., Deshpande, M., Nair, S., Natassia, C., Yordanova, G., Yuan, D., Stroe, O., Wood, G., Laydon, A., et al. (2022). AlphaFold Protein Structure Database: massively expanding the structural coverage of protein-sequence space with high-accuracy models. Nucleic Acids Res. *50*, D439–D444. https://doi.org/10.1093/nar/gkab1061.

71. Jacob, P., Kim, N.H., Wu, F., El-Kasmi, F., Chi, Y., Walton, W.G., Furzer, O.J., Lietzan, A.D., Sunil, S., Kempthorn, K., et al. (2021). Plant "helper" immune receptors are Ca2+-permeable nonselective cation channels. Science *373*, 420–425. https://doi.org/10.1126/science.abg7917.

72. Costes, S.V., Daelemans, D., Cho, E.H., Dobbin, Z., Pavlakis, G., and Lockett, S. (2004). Automatic and quantitative measurement of protein-protein colocalization in live cells. Biophys. J. *86*, 3993–4003. https://doi.org/10.1529/biophysj.103.038422.

73. Schindelin, J., Arganda-Carreras, I., Frise, E., Kaynig, V., Longair, M., Pietzsch, T., Preibisch, S., Rueden, C., Saalfeld, S., Schmid, B., et al. (2012). Fiji: An open-source platform for biological-image analysis. Nat. Methods *9*, 676–682. https://doi.org/10.1038/nmeth.2019.

74. Jumper, J., Evans, R., Pritzel, A., Green, T., Figurnov, M., Ronneberger, O., Tunyasuvunakool, K., Bates, R., Žídek, A., Potapenko, A., et al. (2021). Highly accurate protein structure prediction with AlphaFold. Nature *596*, 583–589. https://doi.org/10.1038/s41586-021-03819-2.

75. Minas, K., Mcewan, N.R., Newbold, C.J., and Scott, K.P. (2011). Optimization of a high-throughput CTAB-based protocol for the extraction of qPCR-grade DNA from rumen fluid, plant and bacterial pure cultures. FEMS. Microbiol. Lett. *325*, 162–169. https://doi.org/10.1111/j.1574-6968.2011.02424.x.

76. Lu, Y., Hatsugai, N., Katagiri, F., Ishimaru, C.A., and Glazebrook, J. (2015). Putative serine protease effectors of clavibacter michiganensis induce a hypersensitive response in the apoplast of nicotiana species. Mol. Plant Microbe Interact. *28*, 1216–1226. https://doi.org/10.1094/MPMI-02-15-0036-R.

77. James, P., Halladay, J., and Craig, E.A. (1996). Genomic Libraries and a Host Strain Designed for Highly Efficient Two-Hybrid Selection in Yeast. Gene *144*, 1425–1436.

78. Ito, H., Mutata, K., and Kimura, A. (1984). Transformation of Intact Yeast Cells Treated with Alkali Cations or Thiol Compounds. Agric. Biol. Chem. *48*, 341–347. https://doi.org/10.1271/bbb1961.48.341.

79. Jacobs, T.B., Zhang, N., Patel, D., and Martin, G.B. (2017). Generation of a collection of mutant tomato lines using pooled CRISPR libraries. Plant Physiol. *174*, 2023–2037. https://doi.org/10.1104/pp.17.00489.

80. French, A.P., Mills, S., Swarup, R., Bennett, M.J., and Pridmore, T.P. (2008). Colocalization of fluorescent markers in confocal microscope images of plant cells. Nat. Protoc. *3*, 619–628. https://doi.org/10.1038/nprot.2008.31.

81. Moschou, P.N., Smertenko, A.P., Minina, E.A., Fukada, K., Savenkov, E.I., Robert, S., Hussey, P.J., and Bozhkov, P.V. (2013). The caspase-related protease separase (EXTRA SPINDLE POLES) regulates cell polarity and cytokinesis in arabidopsis. Plant Cell *25*, 2171–2186. https://doi.org/10.1105/tpc.113.113043.

STAR★METHODS

KEY RESOURCES TABLE

REAGENT or RESOURCE	SOURCE	IDENTIFIER
Antibodies		
anti-flag	Sigma	Cat# F1804; RRID: AB_262044
anti-H^+-ATPase	Agrisera	Cat# AS07 260; RRID: AB_1031584
anti-myc	Cell Signaling Technology	Cat# 2276; RRID: AB_331783
anti-mouse	Cell Signaling Technology	Cat# 7076; RRID: AB_330924
anti-GAL4-TA	Santa Cruz Biotechnology	Cat# sc-510; RRID: AB_627655
anti-GAL4-DBD	Santa Cruz Biotechnology	Cat# sc-1663; RRID: AB_669111
anti-rabbit	Cell Signaling Technology	Cat# 7074; RRID: AB_2099233
anti-RIN4	Gift from Prof. Gitta Coaker, University of California Davis	N/A
anti-goat	Promega	Cat# V8051; RRID: AB_430838
Bacterial and virus strains		
Escherichia coli DH10b	Lab stock	N/A
Escherichia coli Stellar	Lab stock	N/A
Escherichia coli BL21	Lab stock	N/A
Agrobacterium tumefaciens C58C1	Lab stock	N/A
Agrobacterium tumefaciens GV3101	Lab stock	N/A
Agrobacterium tumefaciens AGL-1	Lab stock	N/A
Ralstonia solanacearum GMI1000	Prof. Nemo Peeters (INRA-CNRS)	N/A
Chemicals, peptides, and recombinant proteins		
Phusion® High-Fidelity DNA Polymerase	NEB	Cat# M0530S
BsaI-HF®v2	NEB	Cat# R3733S
T4 DNA Ligase	NEB	Cat# M0202S
Restriction endonucleases for diagnostic digestions	Minotech	Various Catalog numbers (https://minotech.gr/)
Restriction endonucleases for diagnostic digestions	EnzyQuest	Various Catalog numbers (https://enzyquest.com/)
Protease inhibitor cocktail	Sigma-Aldrich	Cat #P9599
Critical commercial assays		
Nucleospin® Gel and PCR Clean-up kit	MACHEREY-NAGEL	Cat# 740609.50
Minute Plasma Membrane Isolation Kit for Plants	Invent Biotechnologies	Cat# SM-005-P
Deposited data		
Mass Spectrometry data of *in vitro* cleavage assays	ProteomeXchange consortium	PXD041406
Experimental models: Organisms/strains		
Saccharomyces cerevisiae PJ69-4A	Prof. Despina Alexandraki (IMBB-FORTH)	N/A
Nicotiana sylvestris TW136	Lab stock	N/A
Nicotiana benthamiana WT	Lab stock	N/A
Nicotiana benthamiana ptr1 mutant plants	Ahn et al. (2023)[69]	N/A
Nicotiana benthamiana nrg1 mutant plants	Qi et al. (2018)[70]	N/A
Nicotiana benthamiana adr1-14 mutant plants	Jacob and Kim et al. (2021)[71]	N/A
Arabidopsis thaliana Col-0	Lab stock	N/A

(*Continued on next page*)

Continued		
REAGENT or RESOURCE	SOURCE	IDENTIFIER
Oligonucleotides		
Oligonucleotide primers	Eurofins Genomics	See Table S2 for details
Recombinant DNA		
Plasmid cloning vectors and plasmid constructs	Variant	See Table S3 for details
Software and algorithms		
Alpha Fold	Varadi et al. (2022)[72] Jumper et al. (2021)[73]	N/A
Dali server	Holm et al. (2020)[63]	http://ekhidna.biocenter.helsinki.fi/dali_server
PyMol molecular graphics system	(The PyMOL Molecular Graphics System, Version 2.0 Schrödinger, LLC)	https://pymol.org/2/
Proteome Discoverer 2.2.0	Thermo Scientific	N/A
Mascot 2.3.02	Matrix Science, London, UK	N/A
LasX (Leica Application Suite X)	Leica Microsystems	RRID:SCR_013673
Fiji	Schindelin et al. (2012)[73]	https://imagej.net/software/fiji/
GraphPad Prism version 8.0.0 for Windows	GraphPad Software, San Diego, California USA	www.graphpad.com
Other		
Immobilon® PVDF membranes	Millipore	Cat# IPVH85R
PureProteomeProtein A/G Magnetic Beads Mix	Millipore	Cat# LSKMAGAG02
Immobilon® ECL Ultra Western HRP Substrate	Millipore	Cat# WBULS0100

METHOD DETAILS

In silico protein structure prediction and analysis

The 3D structure of the full length RipE1 protein was predicted using the AlphaFold Colab.[70,74] Subsequently, the predicted structure was compared with those in the Protein Data Bank via the Dali[49] online server. The visualization of the protein structures was performed by PyMOL (The PyMOL Molecular Graphics System, Version 2.0 Schrödinger, LLC).

Plasmid construction

Genes of interest were amplified using Phusion® High-Fidelity DNA Polymerase (NEB) and PCR products were purified with the Nucleospin® Gel and PCR Clean-up kit (MACHEREY-NAGEL). All constructs used in this study were generated via Golden Gate (GG) Cloning, using the following plasmids as backbone vectors: pGADT7:RFP, pGBKT7:RFP for yeast and pICH86988, pICH86966 for plant assays. RipE1 was amplified from *Ralstonia solanacearum* genomic DNA. *R. solanacearum* GMI1000 was kindly donated by Prof. Nemo Peeters (INRA-CNRS) and gDNA was extracted using the CTAB method.[75] RipE1 mutations were designed according to structural predictions (Figure 1) and recent studies[41,43] and were generated through PCR followed by GG Cloning, using the primers listed in Table S1. Exo70B1, RIN4 and NLR-ID containing constructs were generated as described earlier in a recent study from our lab.[24] pMDC:spC7HPB for *in planta* transient expression of Chp7 was a kind donation of Prof. Jane Glazebrook.[76] Ptr1 was amplified from *Nicotiana benthamiana* cDNA and was cloned in GG-compatible vectors using the primers listed in Table S1. All constructs generated in this study were verified by Sanger sequencing.

Bacterial strains and growth conditions

Escherichia coli (Stellar or DH10b strains) carrying each construct were cultured in LB medium (1% tryptone, 0.5% yeast extract, 1% sodium chloride for liquid cultures and additionally 1,5% agar for plates) containing appropriate antibiotics: ampicillin 100μg/ml or kanamycin 50μg/ml. *E. coli* cells were grown either on LB plates or in liquid LB medium at 37°C for 16h. For liquid cultures, shaking was applied at approximately 200 rpm. *Agrobacterium tumefaciens* (AgL-1, C58C1 or GV3101 strains) were also cultured in LB medium containing appropriate antibiotics: rifampicin 50μg/ml and ampicillin 100μg/ml, kanamycin 50μg/ml or gentamycin 10μg/ml. *R. solanacearum* strain GMI1000 was cultured in NB/NA medium (0.5% tryptone, 0.3% yeast extract, 0.5% sodium chloride for liquid

cultures and additionally 1,5% agar for plates) and grown at 28° for 2 days. For liquid cultures, shaking was applied at approximately 200 rpm.

Y2H assay

All plant proteins were cloned as baits (in the pGBKT7-RFP vector) and bacterial effectors were cloned as preys (in the pGADT7-RFP vector), or as otherwise stated. Different pairs of constructs were co-transformed into *Saccharomyces cerevisiae* strain PJ694a,[77] which carries the following auxotrophic traits: gal4Δ, gal80Δ, trp1-901 leu2-3 ura3-52 his3-200, *LYS2::GAL1-HIS3*, *GAL2-ADE2*, *met2::GAL7-lacZ*. At least 500ng from each plasmid (bait and prey) was used to transform *S. cerevisiae* PJ694a competent cells, freshly prepared with the lithium acetate method.[78] Transformed cells were selected on SD–Leu–Trp medium (SD– LW) agar plates. Two single clones were transferred from the SD–LW medium and were re-cultured on SD–LW (for verification of growth) and SD–Leu–Trp–Ade (–LWA, auxotrophic selection) medium. For the dilutions, a single clone was transferred to liquid SD–LW medium, grown until saturation and diluted as stated in the figures, after OD_{600} measurements. Yeast cells in this study were cultured in YPDA rich medium or SD-LW and SD-LWA minimal media at 28-30°C.

Plant material

The *Nicotiana sylvestris* plants from various ecotypes that were used in our study were grown in greenhouse conditions. For *in planta* transient expression via *Agrobacterium*-mediated infiltration, 4-week-old *N. benthamiana*, 4-week-old *A. thaliana* and 5-week-old *N. sylvestris* TW136 plants were used. For agroinfiltration of *Nicotiana* plants, Agrobacteria carrying indicated constructs were grown in liquid cultures until saturation and cell pellets were diluted in 10mM $MgCl_2$ and 10mM MES. Agrobacteria carrying each construct were then used at an OD_{600} score of 0.5 to infiltrate *N. sylvestris* leaf areas, while agrobacteria carrying empty vector were used to equalize the total OD_{600} score in all inoculums of each experiment. Agroinfiltration in Arabidopsis plants was performed as previously described.[24,69] *Nicotiana benthamiana nrg1* mutants were kindly provided by Jones lab, described in Qi et al. (2018)[59] and the *adr1-14* mutants were kindly provided by Dangl lab, described in Jacob and Kim et al. (2021).[71]

Generation of *Nicotiana benthamiana ptr1* mutant lines using CRISPR/Cas9

Two guide RNAs (NbPtr1-1: gACAAGTATGTTCAGTAAAG and NbPtr1-2: gCAAACACATTCCTTTGTAA) targeting the first exon of *NbPtr1* were designed and cloned into the Cas9-expressing binary vector p201N:Cas9.[79] *N. benthamiana* transformation and molecular characterization of the CRISPR/Cas9-induced mutations in *NbPtr1* were performed as previously described.[61]

Confocal microscopy

All confocal images were captured in a Leica SP8 laser scanning confocal microscope. All leaf tissue samples were imaged with a 40x water objective, after *Agrobacterium*-mediated transient expression at 48-72hpi. The confocal images were processed with ImageJ. For colocalization, all indicated proteins were fused to YFP or mCherry fluorescent epitopes. YFP was excited using a 514-nm argon laser and emission was detected at 520–550 nm. mCherry was excited using a 561-nm laser and emission was detected at 593–628nm. The colocalization analyses were performed with PSC using the Coloc2 addon in Fiji.[80,81] The threshold regression used was Costes, PSF 100 and Costes randomizations 10.[72] A total of 15 regions of interest (ROIs) were chosen for the PSC analysis. For BiFC, all indicated proteins were fused to C-terminal nVENUS or cCFP epitope tags and subsequently, YFP signal was detected. Chlorophyll was detected between 653 and 676 nm and excited at 561 nm. Leica software LASX was used to add scale bars to the images and to display the z-stack maximum projection.

Protein extraction from plant leaf tissue

Agroinfiltrated leaf tissue was ground at 48hpi in liquid nitrogen and proteins were extracted in GTEN buffer (10% glycerol, 25-mM Tris–Cl pH 7.5, 1-mM ethylenediaminetetraacetate, 150-mM NaCl), supplemented with fresh 5-mM DTT, protease inhibitor cocktail (Calbiochem) and 0.15% v/v NP-40, applying vigorous shaking. After a 10-minute centrifugation at high speed (14,000g) at 4°C, the supernatant was collected in a clean microcentrifuge tube and was used for further protein analysis (co-immunoprecipitation, SDS-PAGE and immunoblotting).

Protein extraction from yeast cells

Protein extraction from yeast was done as described earlier.[24]

Co-immunoprecipitation

Protein extract from leaf tissue was incubated for 2h at 4°C with an anti-flag mouse antibody at 1:4,000 dilution (Sigma, F1804), followed by a 1h-incubation at 4°C with PureProteomeProtein A/G Magnetic Beads Mix (Millipore). Beads were washed 3 times with GTEN buffer, before proceeding to SDS-PAGE and immunoblotting.

PM/cell fractionation from plant tissue

PM proteins were extracted using a Minute Plasma Membrane Protein Isolation Kit for Plants (Invent Biotechnologies) as previously described,[24] from *N. sylvestris* tissue transiently expressing proteins of interest (72hpi). H+-ATPase was detected with

an anti-H+ -ATPase (AS07 260; Agrisera) antibody and the cytosolic fraction was verified by staining of the polyvinylidene difluoride (PVDF) membrane with Coomassie Brilliant Blue (CBB) R-250 dye. All fractions obtained via this method were used in immunoblot analysis: the nuclear/chloroplasts and larger debris fraction (N/Chl), the organelle membranes fraction (OM), as well as the cytosolic (C) and plasma membrane (PM) fractions.

SDS PAGE and immunoblotting

Protein samples from plant leaves were prepared for SDS-PAGE electrophoresis by adding 1x SDS loading dye and boiling the samples for 5 min. The samples were then separated via 8% or 12% SDS–PAGE (stated in images captions), electroblotted to a PVDF membrane (Millipore), then blocked for 1h with 5% w/v milk in Tris-buffered saline (TBS; 150-mM NaCl, 50- mM Tris–HCl, pH 7.6) and incubated for 1h with primary antibodies (1:4,000 dilution, anti-flag mouse -Sigma #F1804 or anti-myc mouse -Cell Signaling #2276). Membranes were then incubated for 1h with a secondary antibody (anti-mouse HRP conjugate at 1:10,000 dilution -Cell Signaling) and chemiluminescent substrate ultra (Millipore) was applied for 5 min before camera detection in Sapphire Biomolecular Imager (Azure Biosystems). For protein extracted from yeast cells, PVDF membranes were blocked for 90min with 5% w/v milk in Tris-buffered saline (TBS; 150-mM NaCl, 50- mM Tris–HCl, pH 7.6) containing 0.05% Tween-20 and incubated for 1h with primary antibodies (1:500 dilution, mouse-produced anti-GAL4 TA or anti-GAL4 BD -Santa Cruz Biotechnology). The rest of the procedure was done as with proteins extracted from plant tissue. Relative protein band intensity was measured in Fiji,[73] using the Gel Analysis tool. Measured areas were normalized with CBB staining of Rubisco and submitted to t-tests (as indicated in figure legends) using GraphPad Prism version 8.0.0 for Windows, GraphPad Software, San Diego, California USA (www.graphpad.com).

Protein production and purification

RipE1 gene was cloned and inserted into the pET26b (ColE1 plasmids) vector carrying a C-terminal 6-His tag and transformed into the *E. coli* strain BL21. A sufficient amount of soluble protein was obtained after induction using the following conditions: Cells were grown in LB medium containing 30μg/ml kanamycin until an OD_{600} value of 0.6-0.8 was reached. The culture was induced with 0.5 mM IPTG and left to grow at 20°C overnight. The cell paste was re-suspended in 100 ml lysis buffer containing 25 mM Tris pH 8.0, 300 mM NaCl, 5 mM imidazole and 15 mM β-mercaptoethanol, and homogenized. The cells were disrupted with sonication in ice, 10 sonication cycles of 30 s each, with cooling intervals of 30 s. The precipitate was subsequently removed by centrifugation at 12,000 rpm at 4°C for 45 min. Purification was carried out using His-tag affinity chromatography at 4°C with an 8 ml Ni-NTA Qiagen column pre-equilibrated in lysis buffer and initially washed stepwise with 10, 20 and 30 mM imidazole. With a subsequent increase in imidazole concentration the protein started eluting at 100 mM imidazole. Fractions containing the protein were dialyzed against the storage buffer containing 25 mM Tris pH 8.0, 100 mM NaCl and 10 mM β-mercaptoethanol. In case of EXO70B1, the full-length protein was cloned and inserted into the LIC 1.10 vector carrying a N-terminal 6-His-SUMO3 tag, and transformed into the *E. coli* strain Rosetta™(DE3). The LIC (ligation independent cloning) 1.10 vector carrying the tag was kindly donated by the Netherlands Cancer Institute (NKI). The same protocol was followed and the fractions containing the protein were dialyzed against the storage buffer (25 mM Tris pH 8.0, 100 mM NaCl, 10 mM β-mercaptoethanol and 0.5 nM SENP-2 protease). Subsequently, a reverse purification protocol was carried out using His-tag affinity chromatography. The elution fractions containing the proteins, were polled and concentrated to a final volume of 2 ml. Size exclusion chromatography was performed in 20°C ÄKTA purifier system (Amersham) and a prepacked Hi-Prep 16/60 Sephacryl S-200 high-resolution column (GE Healthcare). Flow rate was 0.5 ml/min, and elution was monitored at 280 nm. Using a 2ml-loop the proteins were loaded, and the 2ml fractions were collected and analyzed via a 10% SDS-polyacrylamide gel.

In vitro cleavage assay

Purified *A. thaliana* Exo70B1 was incubated with purified RipE1 in reaction buffer (25 mM Tris pH 8.0, 100 mM NaCl), for 3 h at room temperature. For the inhibitory assay, RipE1 was incubated with 100 μM leupeptin prior the cleavage assay, at room temperature for 1 h before adding the substrate. After the indicated times, the reaction was stopped by the addition of SDS sample buffer, and the samples were subjected to SDS-polyacrylamide gel electrophoresis and analyzed by Western blotting.

NanoLC-MS/MS analysis

The nanoLC-MS/MS analysis was performed on an EASY-nLC II system (Thermo Scientific) coupled with an LTQ-Orbitrap XL ETD (Thermo Scientific) through a nanoES ion source (Thermo). Data were acquired with Xcalibur software (LTQ Tune 2.5.5 sp1, Thermo Scientific). Prior to the analysis, the mass spectrometer was calibrated with a standard ESI positive ion calibration solution of caffeine (Sigma), L-methionyl-arginyol-phenylalanylalanine acetate H2O (MRFA, Research Plus, Barnegat, NJ), and perfluoroalkyl triazine (Ultramark 1621, Alfa Aesar, Ward Hill, MA). Samples were reconstituted in 0.5% formic acid, and the tryptic peptide mixture was separated on a reversed-phase column (Reprosil Pur C18 AQ, particle size = 3 μm, pore size = 120 Å (Dr. Maisch, AnaLab, Athens, Greece), fused silica emitters 100 mm long with a 75 μm internal diameter (New Objective) packed in-house using a pressurized (35 to 40 bars of helium) packing bomb. The nanoLC flow rate was 300 nl min−1. The LC mobile phase consisted of 0.5% formic acid in water (A) and 0.5% formic acid in acetonitrile (B). A multi-step gradient was employed, from 5% to 30% B in 120 min, to 90% B in 10 min. After the gradient had been held at 90% B for 5 min, the mobile phase was re-equilibrated at initial gradient conditions. The MS was operated with a spray voltage of 2300 V, a capillary voltage of 35 V, a tube lens voltage of 140 V, and a capillary temperature

of 180°C. A survey scan was acquired in the range of m/z 400–1800 with an AGC MS target value of 106 (resolving power of 60,000 at m/z 400). The 10 most intense precursor ions from each MS scan were subjected to collision-induced dissociation in the ion trap. The mass spectrometry proteomics data have been deposited to the ProteomeXchange Consortium via the PRIDE[68] partner repository with the dataset identifier PXD041406.

Data analysis of MS/MS-derived data

The MS raw data were loaded in Proteome Discoverer 2.2.0 (Thermo Scientific) and run using Mascot 2.3.02 (Matrix Science, London, UK) search algorithm against the EXO70B1 Sequence. A list of common contaminants was included in the database. For protein identification, the following search parameters were used: precursor error tolerance = 10 ppm, fragment ion tolerance = 0.8 Da, no enzyme specificity, maximum number of missed cleavages = 3, and cysteine alkylation as a fixed modification, Oxidation of Methionine, Acetylation of N-term, Phosphorylation (The node ptmRS was used) of Serine, Threonine and Tyrosine as Variable Modifications. To calculate the protein false discovery rate, a decoy database search was performed simultaneously with strict criteria set to 0.01 and relaxed criteria to 0.05.

Statistical analysis and plotting of hypersensitive response (HR) assay results

Statistical analysis and plotting were performed using GraphPad Prism version 8.0.0 for Windows, GraphPad Software, San Diego, California USA (www.graphpad.com). For HR assays, a score 0-5 was assigned to each observed phenotype, representing cell death intensity. HR scores from 12 replicates were submitted to t-test followed by Welch's correction. Differences with p value <0.05 were considered statistically significant (*), while multiple asterisks were used to indicate profoundly low p value (as stated in the corresponding figure legends).

RIN4 degradation assay

Agrobacterium tumefaciens GV2260 expressing the effector genes of interest was grown on LB media with the appropriate antibiotics for 2 days at 30°C. Bacteria were scraped from the plate, resuspended in infiltration buffer (10 mM MgCl2, 10 mM morpholineethane sulfonic acid [pH 5.6], and 200 mM acetosyringone), and were maintained for 3h at room temperature on a shaker. Bacterial cultures were then washed and centrifuged, and the pellet was resuspended in fresh infiltration buffer before diluting cultures at a final OD_{600} of 0.2. Bacterial solution was syringe infiltrated into 5-week-old *N. benthamiana* leaves and leaf samples for protein expression were taken 46 h later. Total protein was extracted from a pool of discs from three *N. benthamiana* plants using 250 μL extraction buffer consisting of 50 mM Tris HCl [pH 7.5], 10% glycerol, 2% SDS, 2 mM EDTA, 1 mM dithiothreitol, and 1% protease inhibitor (Sigma-Aldrich). Total protein was subjected to immunoblotting using α-RIN4 antibody (gift from G. Coaker, University of California Davis) at a concentration of 1:2,000. Secondary goat antirabbit immunoglobulin G conjugated with HRP was used at a dilution of 1:10,000 (Promega).

Agrobacterium-mediated hairpin-based silencing

Silencing of *Nb*Ptr1 was performed via an *Agrobacterium*-mediated hairpin system, according to Brendolise et al.[60], where agroinfiltrations were performed in two subsequent days. The first day, the two right patches were infiltrated with agrobacteria carrying the hairpin construct (hp), while the two left patches with agrobacteria carrying the corresponding empty vector (EV). The following day, the two upper patches were infiltrated with agrobacteria carrying the effector construct, while the two bottom patches with agrobacteria carrying the corresponding empty vector. All constructs were infiltrated at OD_{600} of 0.5. Photographs were taken 3 days after effector infiltration.